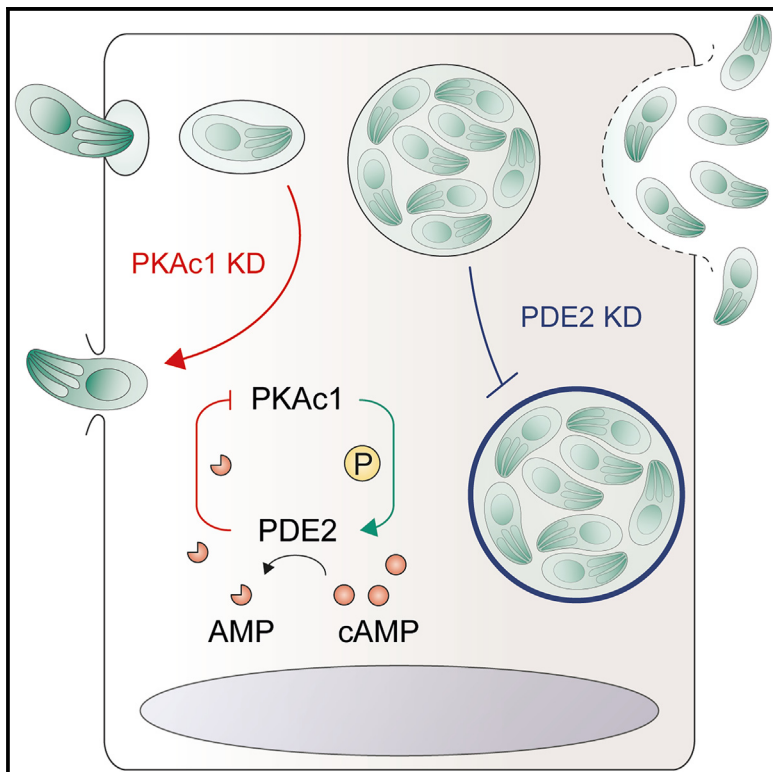


Phospho-relay feedback loops control egress vs. intracellular development in *Toxoplasma gondii*

Graphical abstract



Authors

Ja E. Claywell, Yong Fu, L. David Sibley

Correspondence

sibley@wustl.edu

In brief

Claywell et al. show that *Toxoplasma* egress is controlled by a negative feedback loop. PKAc1 is activated after invasion to inhibit egress by targeting processes between cGMP production and Ca^{2+} signaling. PKAc1 activation of PDE2 serves to deplete cAMP, thus downregulating PKAc1 activity and permitting egress through the PKG/CDPK pathway.

Highlights

- Protein kinase Ac1 inhibits egress in *Toxoplasma* by suppressing calcium signaling
- Adenylate cyclase AC α 3 and phosphodiesterase 2 control cAMP to regulate PKAc1
- PKAc1 phosphorylates PDE2 to cleave cAMP and form a negative feedback loop
- PKAc1 acts on targets between cGMP and calcium release to prevent egress



Article

Phospho-relay feedback loops control egress vs. intracellular development in *Toxoplasma gondii*

Ja E. Claywell,¹ Yong Fu,¹ and L. David Sibley^{1,2,*}

¹Department of Molecular Microbiology, Washington University School of Medicine, 660 S. Euclid Avenue, St. Louis, MO 63110, USA

²Lead contact

*Correspondence: sibley@wustl.edu

<https://doi.org/10.1016/j.celrep.2025.115260>

SUMMARY

The intracellular parasite *Toxoplasma gondii* alternates between a motile invasive and a quiescent intracellular replicative form, yet how these transitions are regulated is unknown. A positive feedback loop involving protein kinase G (PKG) and calcium-dependent PKs (CDPKs) controls motility, invasion, and egress by *Toxoplasma gondii*, while PKA isoform c1 (PKAc1) counteracts this pathway. Shortly after invasion, PKAc1 is activated by cyclic AMP (cAMP) produced by adenylate cyclases, leading to the suppression of the PKG/CDPK pathway. PKAc1 further activates phosphodiesterase 2, which selectively consumes cAMP, thus forming a negative feedback loop, causing transient activation of PKAc1. Perturbation of cyclic GMP (cGMP) vs. calcium demonstrates that PKAc1 acts on targets between guanylate cyclase and calcium release. The combined activation of PKG/CDPKs and inhibition by PKAc1, controlled by a transient negative feedback loop, ensures that the parasite is responsive to environmental signals needed to activate motility while also ensuring periods of long-term stable intracellular growth.

INTRODUCTION

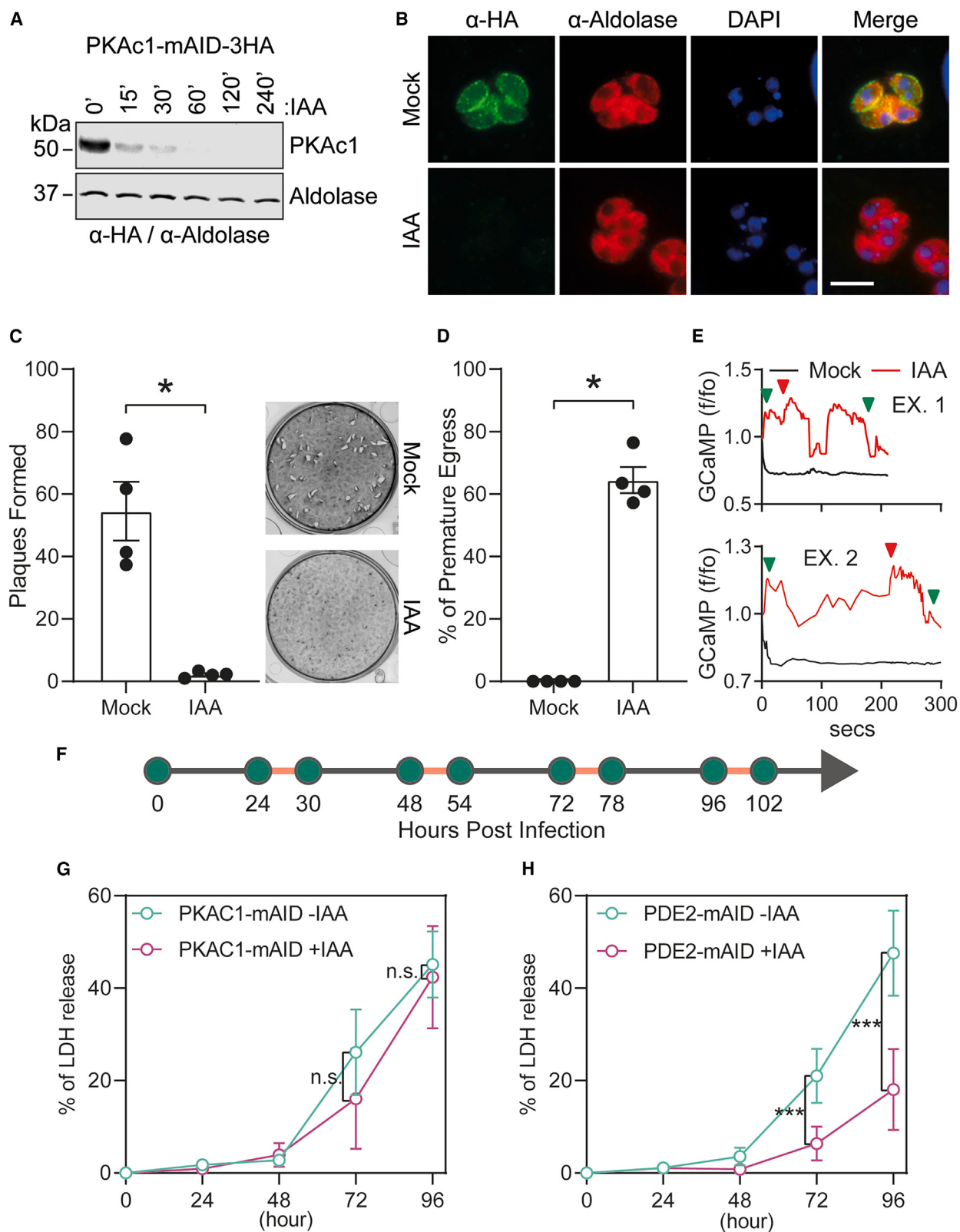
Toxoplasma gondii is an obligate intracellular parasite that is capable of infecting virtually any nucleated cell in a wide variety of warm-blooded animals and causing disease in humans and animals worldwide.¹ Host cell invasion occurs by gliding motility, apical attachment that is mediated by secreted adhesins, and penetration to generate a parasitophorous vacuole.^{2,3} Following invasion, the parasite suppresses calcium signaling and motility and remains quiescent while undergoing multiple rounds of division prior to activating motility to egress and continue the lytic cycle.⁴ During acute infection, multiple rounds of this lytic cycle are responsible for parasite expansion and dissemination. Although some of the key players in this process are defined, how the parasite coordinates the switch between active protein secretion and motility vs. quiescent intracellular replication is poorly understood.

Prior studies have shown that active motility, invasion, and egress of *T. gondii* tachyzoites are controlled by a protein kinase G (PKG) pathway^{5,6} in concert with elevated calcium and activation of calcium-dependent PKs (CDPKs).⁷ This cascade is initiated by the action of a membrane-associated guanylate cyclase (GC) that generates cGMP to activate PKG.^{8–10} Among its downstream targets, PKG stimulates the release of calcium from intracellular stores¹¹ and likely also facilitates uptake from the extracellular environment.¹² Studies in the related apicomplexan parasite *Plasmodium falciparum* indicate that calcium responses, CDPKs, and motor proteins are all downstream targets

of PKG.¹³ The use of calcium reporter strains treated with the phosphodiesterase (PDE) inhibitor zaprinast also implicates PKG in controlling calcium release in *T. gondii*.^{14,15} This pathway further depends on an AGC kinase called store potentiating and activating kinase (SPARK), which is required for the PKG-dependent release of intracellular calcium.¹⁶ Elevated calcium in *T. gondii* actives CDPK1 and CDPK2A, which regulate microneme secretion and adhesin deployment.^{17–19} Further studies have shown that CDPK1, CDPK3, and PKG interact in a positive feedback loop to promote calcium-dependent protein secretion and motility, which are required for both invasion and egress from host cells.^{20–23} Elevated calcium is also needed to facilitate membrane docking of micronemes in a process that is mediated by proteins bearing calcium-binding elements such as DOCK²⁴ and FER2.²⁵ Imaging of calcium in motility in tachyzoites reveals oscillating cycles of elevated calcium associated with gliding motility²⁶ and cell attachment.²⁷ Remarkably, these signals are rapidly quenched when a parasite invades its host cell.¹¹ In late-stage vacuoles, calcium levels are again elevated, leading to microneme secretion, motility, and egress.²⁸

T. gondii contains three isoforms of PKA, and previous studies have shown that PKAc3 (TGME49_286470) is involved in negatively regulating bradyzoite differentiation,²⁹ while PKAc2 (TGME49_228420) is primarily expressed during merogony in the cat gut.^{30,31} In contrast, previous studies have implicated PKAc1 (TGME49_226030) in *T. gondii* as a negative regulator of the PKG pathway. Expression of a dominant-negative form of the regulatory subunit PKAr (TGME49_242070) that does not





(legend on next page)

bind cyclic AMP (cAMP) or genetic depletion using a tetracycline-off system led to “restless invasion” that did not result in the establishment of parasitophorous vacuoles that support parasite replication.³² Another group using the tetracycline-off system extended these findings by showing that newly invaded parasites undergo premature egress associated with an inability to quench calcium levels following invasion.³³ Although these studies indicate that PKG and PKAc1 drive opposing pathways, they do not reveal how PKAc1 is regulated, what activates it, or how it is ultimately shut off to allow de-repression of the PKG pathway.

Previous studies examining the PKAc1-dependent phosphoproteome identified several putative targets in the PKG pathway,³² although these studies did not provide a mechanistic link for how the pathways are interrelated. Additionally, this study identified PDE2 (TGME49_293000) as a putative PKAc1-dependent substrate.³² Here, we explore the interaction between PKAc1 and PDE2 and show that they form a negative feedback loop that suppresses the PKG pathway and ensures homeostatic control during intracellular development.

RESULTS

Conditional degradation of PKAc1 activates premature egress

Here, we utilized the mini auxin-inducible degron (mAID) system^{34,35} to study dynamic signaling pathways controlled by this kinase. We introduced a mAID-3HA tag to the C terminus of PKAc1 and tested its degradation in ME49 Tir1-3FLAG parasites (Figures S1A and S1B). The addition of auxin promoted the efficient knockdown of PKAc1-mAID-3HA following 60 min treatment, as shown by western blotting (Figure 1A) and immunofluorescence (IF) microscopy (Figure 1B). Moreover, PKAc1-mAID-3HA localized to the periphery of the parasite, indicating that the mAID-3HA tag does not interfere with its interaction with the in-

ner membrane complex (IMC)-associated regulatory subunit PKAr, which is targeted to the membrane (Figure 1B). Consistent with its role as a negative regulator of egress, plaque formation assays revealed that PKAc1-depleted parasites exhibited a severe lytic growth defect compared to parasites expressing PKAc1 (Figure 1C).

Next, we sought to confirm previously published PKAc1 phenotypes using the more rapid degradation afforded by the mAID system. Since Ca²⁺ signaling has been shown to play an integral role in egress, we stably introduced the calcium reporter GCaMP6f at the HXGPRT locus into the parental line, ME49 PKAc1-mAID-3HA, to monitor Ca²⁺ levels during invasion and egress (Figures S1C and S1D). The degradation of PKAc1-mAID-3HA with indole acetic acid (IAA) did not alter protein levels or cytosolic localization of GCaMP6f in parasites based on western blot analysis and IF microscopy (Figures S1E and S1F). In order to explore its role in early events, PKAc1-mAID-3HA, GCaMP parasites grown ± IAA were harvested and then used to challenge fresh human foreskin fibroblast (HFF) monolayers. PKAc1-mAID-3HA-depleted parasites efficiently invaded cells, but 64% subsequently egressed within 15 min, whereas 100% of invaded parasites expressing PKAc1 remained within the cell (Figure 1D). Additionally, Ca²⁺ levels continued to oscillate in PKAc1-mAID-3HA-depleted parasites compared to parasites expressing PKAc1, where calcium levels were suppressed following invasion. In addition to early egress, natural egress at later stages of infection was examined in PKAc1-mAID-3HA parasites grown continuously in the presence of IAA after invasion (Figure 1F). Knockdown of PKAc1 did not induce egress at later time points, indicating that PKAc1 is critical during early infection but dispensable at later time points (Figure 1G).

Role of ACs in controlling PKAc1

PKA is normally kept in an inactive conformation by binding to a regulatory subunit PKAr.³⁶ PKA becomes activated when cAMP,

Figure 1. Conditional degradation of PKAc1 leads to loss of calcium dampening and premature egress

- (A) Western blot analysis of PKAc1-mAID-3HA parasites treated with indole acetic acid (IAA; 500 μM) or diluent (0.1% ethanol) for various times shown in min (''). Immunoblots were probed with antibodies recognizing the HA epitope (α -HA) and *T. gondii* aldolase (α -aldolase), followed by IR dye-conjugated secondary antibodies. A representative blot from at least two independent experiments is shown. See also Figures S1A and S1B.
- (B) IF analysis of PKAc1-mAID-3HA-infected HFF cells at 24 h post-infection (hpi) following 1 h treatment with IAA (500 μM) or diluent (0.1% ethanol). Cells were fixed, stained with the antibodies indicated, and detected with Alexa Fluor-conjugated secondary antibodies. Representative images from at least two independent experiments are shown. Scale bar: 5 μm.
- (C) Plaque formation of PKAc1-mAID-3HA parasites following growth in the presence of IAA (500 μM) or diluent (0.1% ethanol) for 14 days. Means ± SE from at least three independent experiments are shown. Unpaired Student's t test (mock vs. IAA) (* p < 0.05).
- (D and E) Egress and Ca²⁺ signaling in PKAc1-mAID-3HA, GCaMP parasites.
- (D) Egress assay of IAA (500 μM) or diluent (0.1% ethanol) treated PKAc1-mAID-3HA, GCaMP parasites (treated overnight, harvested, and added to monolayers). Premature egress was calculated as a percentage of parasites that egressed within 15 min. Means ± SE from at least four independent experiments are shown. Unpaired Student's t test (mock vs. IAA) (* p < 0.05). Invasion was noted as T = 0, and each parasite was subsequently monitored for 15 min. See also Figures S1C–S1F.
- (E) GCaMP fluorescence profiles of PKAc1-mAID-3HA, GCaMP parasites treated with IAA (500 μM) or diluent (0.1% ethanol). Data represent the relative intensity of GCaMP fluorescence fold change (f/f₀) from a single parasite vs. time from at least three independent experiments. Each parasite was monitored just prior to invasion (T = 0) up to at least 2 min. Two representative GCaMP profiles are shown. Green and red arrows denote just before invasion or reinvasion into a new cell and egress, respectively, for parasites exhibiting premature egress.
- (F) Illustration of monitoring the spontaneous egress. Lactate dehydrogenase (LDH) activity was measured in cell supernatant collected 6 h post-lysis at each time point.
- (G and H) HFFs were infected with PKAc1-mAID (G) and PDE2-mAID (H) ± 500 μM IAA treatment for 0, 24, 48, 72, and 96 h. Cell supernatant was collected 6 h post-lysis at each time point, and LDH activity was determined to measure cell lysis. LDH release was calculated as a percentage of maximal release (post-Triton treatment of non-infected cells). Data were pooled from three independent experiments, mean ± SD (n = 3 experiments, each with three technical replicates per treatment). Multiple Student's t tests, *** p < 0.001, n.s., not significant.

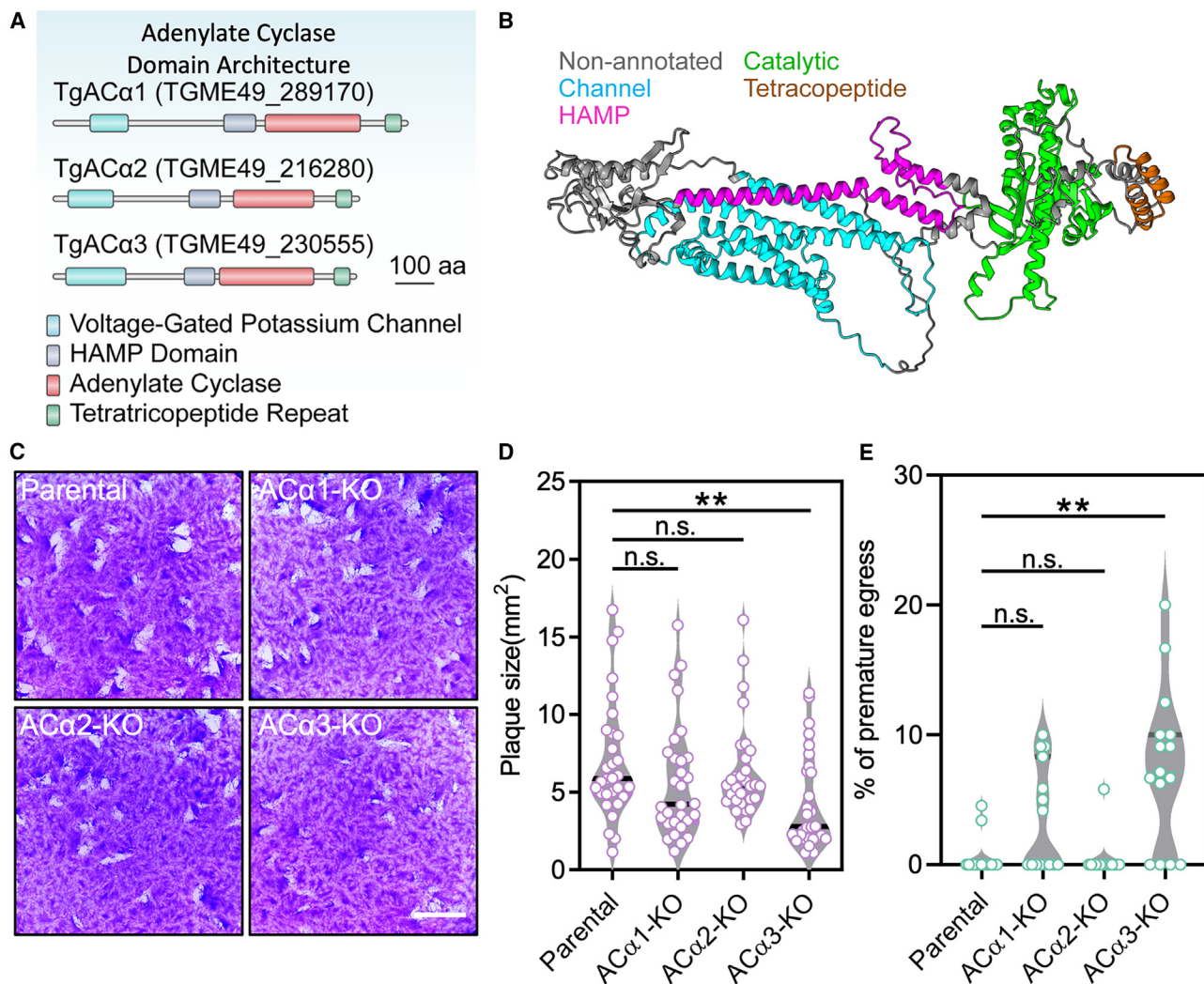


Figure 2. Domain structure and functional role of ACs in *T. gondii*

(A) Domain structures of three adenylate cyclases (ACs) in *T. gondii* with gene IDs from ToxoDB.

(B) Model of *T. gondii* AC3 generated by AlphaFold (<https://alphafold.ebi.ac.uk/>) and visualized using Chimera X.⁴¹ Domain structures are based on homology modeling using the MPI Bioinformatics Toolkit webserver.⁴²

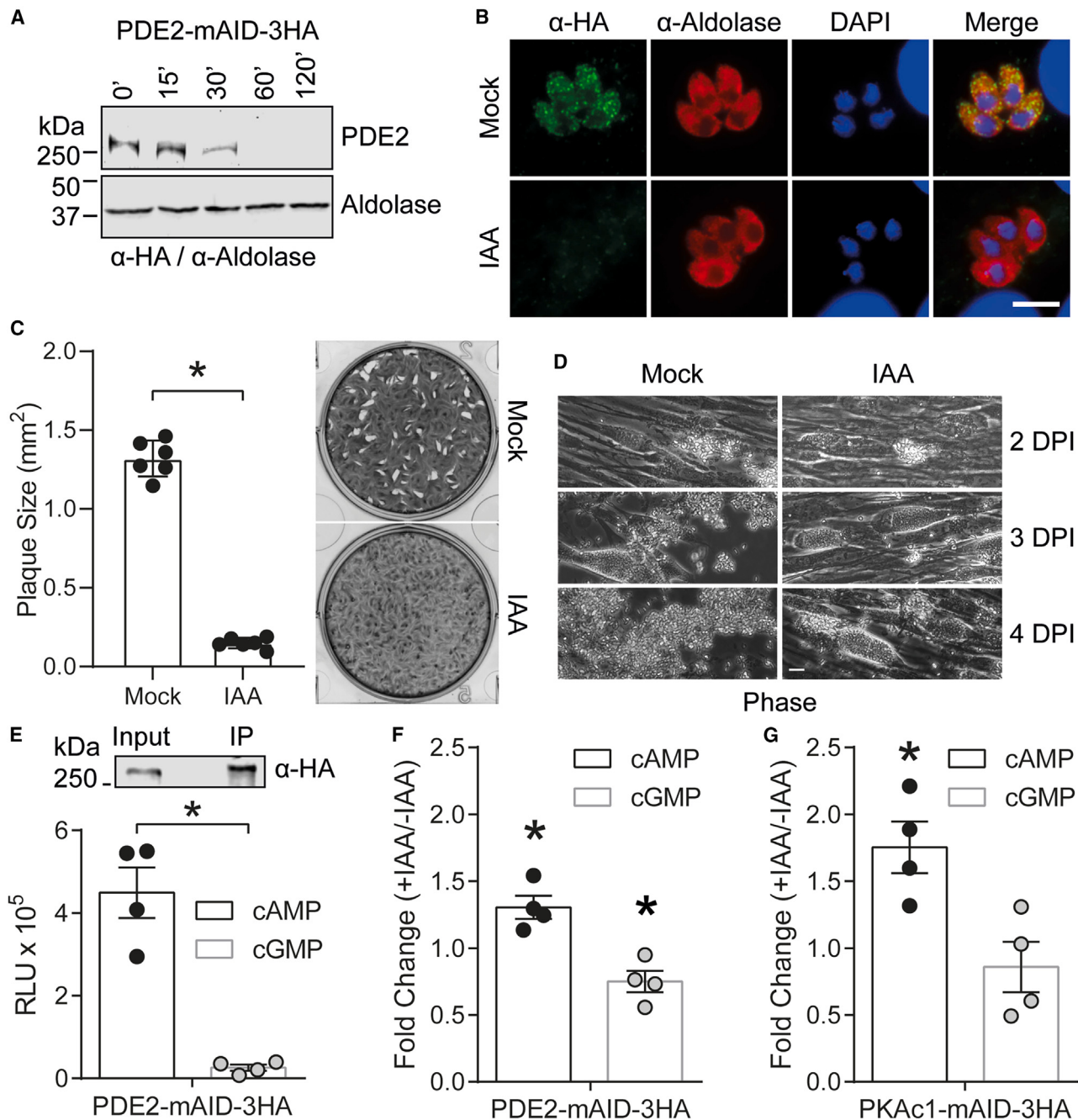
(C) Plaque assay of AC-knockout parasites grown onto HFFs for 14 days. Scale bar: 5 mm.

(D) Quantification of the area of plaques formed in (C). Data are represented as mean \pm SD and plotted from two independent assays with 15 replicates for each ($N = 2, n = 30$). One-way ANOVA with Dunn's multiple comparison correction test. n.s., not significant, ** $p < 0.01$.

(E) Quantification of premature egress of AC-knockout parasites using time-lapse imaging over 5 min following the initial invasion. Means \pm SD from two independent assays with biological 8 replicates for each are shown ($N = 2, n = 16$). One-way ANOVA with Dunn's multiple comparison correction test. n.s., not significant, ** $p < 0.01$.

produced by adenylate cyclase (AC), binds to cAMP response elements in PKAr to release the kinase.³⁶ Previous studies in *T. gondii* identified a single AC β that is involved in rhoptry biosynthesis³⁷ and a single AC α 1 that showed only a mild phenotype when disrupted.³² We re-examined the genome of *T. gondii* and identified three isoforms, named here as AC α 1 (corresponding to the previously studied gene), AC α 2, and AC α 3 (Figure 2A). Somewhat unusually, these ACs contain a predicted N-terminal voltage-gated K channel followed by a long α -helical HAMP domain (named for histidine kinases, ACs, methyl-accepting proteins, and phosphatases)³⁸ and then the AC domain followed

by a tetrastricopeptide repeat (TPR) domain (Figure 2B). HAMP domains regulate activity by transducing signals from membrane receptors to catalytic domains in the cytosol, whereas TPR domains serve to facilitate protein-protein interactions by acting as scaffolds.^{39,40} The role of these domains in *T. gondii* ACs is uncertain, but their arrangement suggests that external signals are transduced to activate the catalytic function. We deleted each of the genes using CRISPR-Cas9 gene editing to replace the coding region with a selectable marker (Figures S2A-S2C). Plaquing of the knockout clones in comparison to wild-type (WT) parasites revealed a mild phenotype for AC α 3, which

**Figure 3. PDE2 regulates lytic growth by controlling cAMP levels**

(A) Western blot analysis of PDE2-mAID-3HA parasites probed with α -HA or α -aldolase primary antibodies followed by IR dye-conjugated secondary antibodies. See also Figures S2A and S2B.

(B) IF microscopy of PDE2-mAID-3HA parasites at 24 hpi following treatment with IAA (500 μ M) or diluent (0.1% ethanol) for 1 h. Intracellular parasites were labeled with primary antibodies and detected with Alexa Fluor-conjugated secondary antibodies. Representative images from at least two independent experiments are shown. Scale bar: 5 μ m.

(C) Plaque formation of PDE2-mAID-3HA parasites grown in the presence of IAA (500 μ M) or diluent (0.1% ethanol) for 14 days. Means \pm SE from at least six independent experiments. Unpaired Student's t test (mock vs. IAA) ($*p < 0.05$). See also Figure S2C.

(D) Natural egress of PDE2-mAID-3HA parasites treated with IAA (500 μ M) or diluent (0.1% ethanol) for 4 days. Representative images from at least three independent experiments are shown.

(legend continued on next page)

formed similar numbers of plaques (Figure S2E) that were significantly smaller (Figure 2C). We also examined the knockout clones by video microscopy to monitor premature egress during the first 5 min after invasion of freshly harvested tachyzoites. The AC α 1 knockout showed a slight elevation in premature egress that was not significant, while elevated egress observed in the AC α 3 knockout was statically significant (Figure 2D). These results suggest that AC α 3 is primarily responsible for generating cAMP and activating PKAc1, as its absence partially phenocopies the conditional knockdown of PKAc1.

PDE2 is required for egress and negatively regulates PKAc1

Previous studies investigating the altered phosphorylation of proteins in the absence of PKAc1 identified several potential substrates downstream of this kinase.³² Among these substrates, PDE2 has been implicated in cAMP signaling and egress^{23,43,44} and is one of two essential PDEs of 18 encoded in the *T. gondii* genome.^{43,45} To investigate the role of PDE2, we introduced a mAID-3HA to the C terminus of PDE2 using CRISPR-Cas9 editing (Figures S3A and S3B). The knockdown of PDE2-mAID-3HA was rapid and efficient, with protein levels being undetectable after a 60 min treatment with IAA (Figure 3A). PDE2-mAID-3HA localized to punctate structures within the cytosol, and a 60 min treatment with IAA led to a significant decrease in PDE2-mAID-3HA levels (Figure 3B), consistent with the degradation kinetics determined by western blot analysis (Figure 3A). Although PDE2-mAID-3HA-depleted parasites could form plaques, the average size of plaques was significantly reduced in comparison to parasites expressing PDE2-mAID-3HA, indicating that proper control of cyclic nucleotide monophosphate (cNMP) levels are critical for lytic growth (Figures S3C and 3C). Consistent with the plaquing defect, the conditional knockdown of PDE2 led to a delay in natural egress. When visualized by microscopy, enlarged vacuoles containing many intracellular parasites were observed at late time points, when the majority of mock-treated parasites had egressed (Figure 3D). Quantification of this defect using lactate dehydrogenase release from the host cytosol revealed a pronounced defect at 72 and 96 hpi (Figure 1H). These data indicate that the loss of PDE2 impairs natural egress at the end of the intracellular growth cycle.

The defects in natural egress prompted us to hypothesize that PDE2 may regulate egress by controlling the activity of PKAc1. Since PKAc1 is activated by cAMP, turnover of this cyclic nucleotide would be a potent mechanism for inhibition. To determine substrate specificity, PDE2-mAID-3HA was immunoprecipitated from *T. gondii* tachyzoite lysates and assayed for activity using cAMP or cGMP as substrates. PDE2-mAID-3HA exhibited strong activity toward cAMP but little to no activity toward cGMP (Figure 3E), indicating that PDE2 is a cAMP-specific

PDE, consistent with previous reports.^{23,43,44} The impact of the loss of PDE2 vs. PKAc1 on intracellular cyclic nucleotide (cNMP) levels was also examined using ELISA-based assays. The conditional knockdown of PDE2 led to elevated levels of cAMP levels, consistent with its role as a cAMP-specific PDE (Figure 3F), with a slight decrease in cGMP. Interestingly, the depletion of PKAc1-mAID-3HA also led to a rise in cAMP levels but little to no change in cGMP levels (Figure 3G). The rise in cAMP levels following the loss of PKAc1-mAID-3HA suggests a possible feedback loop with PDE2.

PKAc1 phosphorylates PDE2 at multiple sites

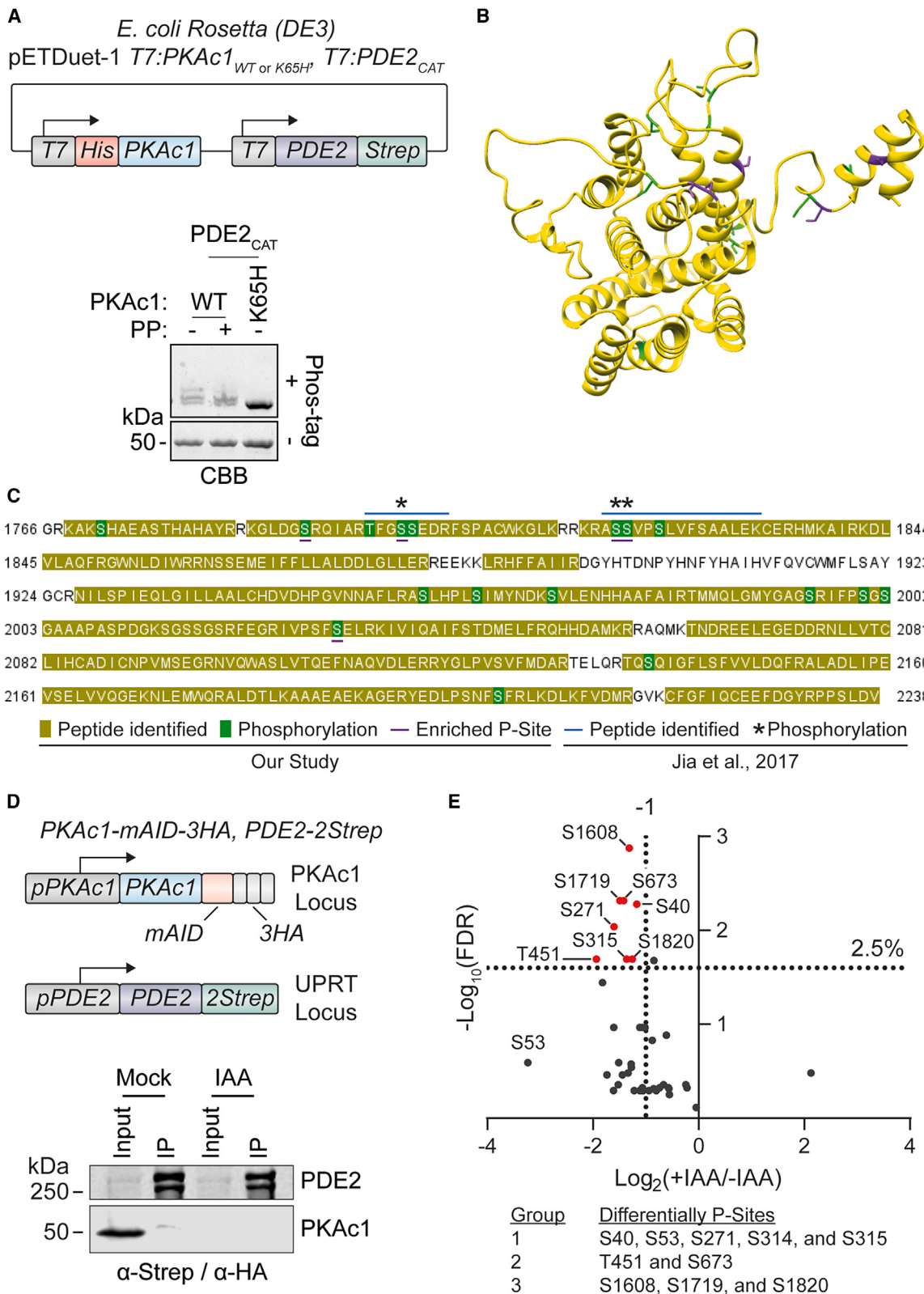
To determine whether PDE2 serves as a substrate for PKAc1, we co-expressed the catalytic domain of PDE2 (PDE2_{CAT}) with either active PKAc1 or an inactive form of PKAc1 harboring a K65H point mutation in *E. coli*. We then assessed the phosphorylation of PDE2 using Phos-tag gels, which detect phosphorylation by mobility shift (Figure 4A). When co-expressed with the active form of PKAc1, PDE2_{CAT} resolved as a triplet, indicating multiple phosphorylated species (Figure 4A). In contrast, co-expression of PDE2_{CAT} with the active form of PKAc1 followed by lambda phosphatase treatment resulted in faster migration of a single species in Phos-tag gels (Figure 4A). PDE2_{CAT} co-expressed with the inactive form of PKAc1 also migrated as a single distinct band with faster mobility, consistent with a lack of phosphorylation (Figure 4A).

After verifying that PKAc1 phosphorylates PDE2_{CAT} *in vitro*, mass spectrometry (MS) was used to identify phosphorylation sites in PDE2_{CAT} following co-expression with either the active or inactive form of PKAc1. Post-translational modification analysis of tandem MS (MS/MS) spectra revealed the presence of 17 unique P-Ser/P-Thr residues that were absent in PDE2_{CAT} co-expressed with the inactive form of PKAc1 (Figures 4B and 4C). The phosphorylated sites were mapped on a predicted Swiss homology model of PDE2_{CAT} (Figure 4B), and the top five enriched phosphorylated residues based on differences in spectral counts included S1820, S1819, S1790, S1799, and S1995 (Figure 4C). The designated residues were phosphorylated at a ratio of at least 1:20 (phosphorylated peptide vs. non-phosphorylated peptide), with S1820 and S1829 being the most phosphorylated, with ~50% of all peptides being phosphorylated. Three of the residues detected here, S1799, S1819, and S1820, were found to be phosphorylated in previous work,^{32,46} suggesting they may serve a role in regulating PDE2 (Figure 4C).

Recognizing that co-expression in a heterologous system might lead to permissive phosphorylation, we also examined the phosphorylation of PDE2 in *T. gondii*. We generated a line in which PDE2 was twin-strep tagged at the C terminus to allow affinity purification in a PKAc1-mAID-3HA background (Figures S4A, 4B, and 4D). Purified PDE2-2Strep was obtained from

(E) PDE assay of immunoprecipitated PDE2-mAID-3HA using 1 μ M cAMP or 10 μ M cGMP performed at 30°C for 1 h. Mean RLU \pm SE from at least three independent experiments is shown. Western blot analysis of input and immunoprecipitation (IP) samples using α -HA primary antibodies and Alexa Fluor-conjugated secondary antibodies is shown.

(F and G) Cytoplasmic cyclic nucleotide levels of purified PDE2-mAID-3HA (F) and PKAc1-mAID-3HA (G) parasites treated with IAA (500 μ M) or diluent (0.1% ethanol) determined by ELISA. Fold change = ratio of cNMP levels in the IAA-treated sample vs. ethanol-treated sample. Average fold change \pm SE from at least four independent experiments. Unpaired Student's t test (fold change vs. 1) (* p < 0.05).



(legend on next page)

parasites cultured in the presence or absence of IAA to degrade PKAc1 and then submitted for MS to identify differentially phosphorylated residues. The MS analysis identified an abundance of phosphorylated residues, with eight sites showing significantly reduced phosphorylation intensities when PKAc1 was knocked down (Figure 4E). In addition to the previously identified residues in the C-terminal catalytic domain, several phosphorylated residues were clustered toward the N terminus. Residues S53 and S314 were also of interest due to their significant fold reduction in phosphorylation intensity following PKAc1 knockdown and their proximity to S315, respectively (Figure 4E). Of these sites, S1820 was previously identified by others³² and also seen in the pDuet system above, while the majority of sites found in the N terminus that were not included in the studies in *E. coli*. To better understand the consequence of phosphorylation on the structure/function of PDE2, the eight differentially phosphorylated residues were mapped onto a predicted AlphaFold model of PDE2 (Figure S4C). These residues, except for S1820, mapped to unstructured regions with no obvious domain structure. To facilitate downstream testing, phosphosites were categorized into three groups based on their proximity to each other in the linear sequence: group 1 consisted of S40, S53, S271, S314, and S315, group 2 contained T451 and S673, and group 3 included S1608, S1719, and S1820 (Figure 4E). Sequence logo analysis of phosphosites identified in PDE2 indicated a PKAc1 phosphorylation motif of RXXS/TP (Figure S4D*i*). This motif is consistent with the PKAc1 phosphorylation motif generated from PDE2 phosphosites in the Jia et al. study³² (Figure S4D*ii*).

PDE2 harboring phospho-mutations alter enzymatic activity and delay parasite egress

Because PKAs are known to regulate the enzymatic activity of PDEs in other model systems,^{47,48} we tested whether PKAc1-dependent phosphorylation sites alter the activity of PDE2. We interrogated the function using phospho-mimetic amino acid substitutions that mimic (aspartic acid [D] for serine [S] and glutamic acid [E] for threonine [T]) or ablate (alanine [A] for S or T) phosphorylation at specific residues. We reasoned that if PDE2 activity is dependent on phosphorylation, then amino acid substitutions that mimic phosphorylation at PKAc1-dependent sites would express constitutive PDE2 activity, whereas amino acid substitutions that ablate phosphorylation would block PDE2 activity. This prediction is based on the observation that the knockdown of PKAc1 led to higher cytosolic cAMP levels, suggesting

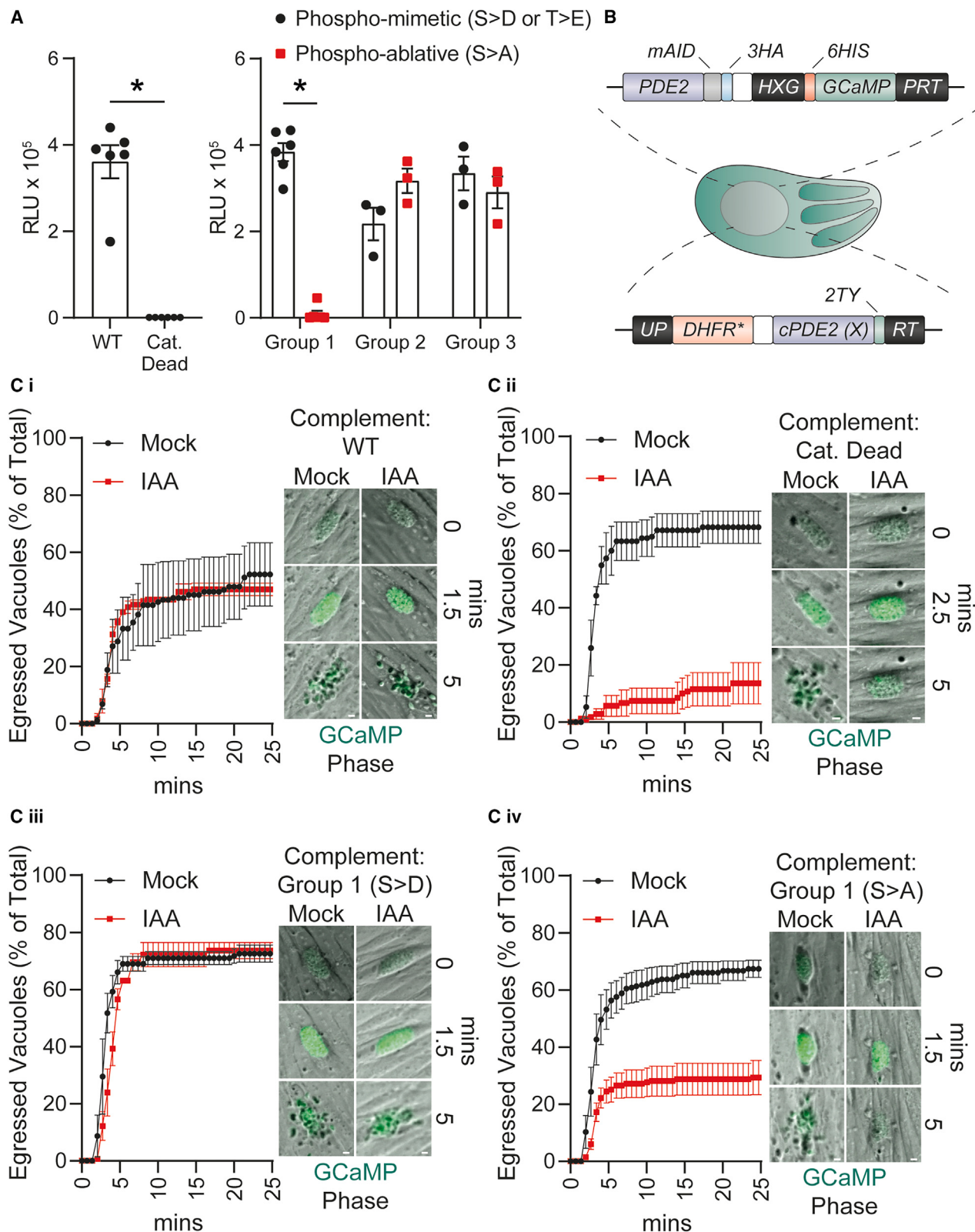
that PKAc1 phosphorylation of PDE2 likely activates the enzyme to cleave cAMP (Figure 3G). We affinity purified twin-strep-tagged PDE2 (rPDE2) harboring either phospho-mimetic (S>D or T>E) or phospho-ablative (S/T>A) mutations at key positions from HEK293T cells (Figures S5A and S5B). We focused on residues that were differentially phosphorylated based on statistical analysis in addition to S53 and S314 (Figure 4E). PDE2 proteins bearing substitutions that were clustered into three groups were expressed HEK293T cells, affinity purified (Figures S5A and S5B), and tested for their ability to hydrolyze cAMP. Consistent with assays performed with PDE2 immunoprecipitated from parasite lysates (Figure 3E), WT rPDE2 exhibited activity toward cAMP, indicating it is activated in this heterologous system (Figure 5A). In contrast, H1994A and D1945A mutations that lie in the catalytic site abrogated activity (Figure 5A). PDE activity toward cAMP of phospho-mimetic and -ablative forms of rPDE2 harboring mutations in group 2 (e.g., T451 and S673) as well as group 3 (e.g., S1608, S1719, and S1820) did not significantly change activity (Figure 5A). In contrast, phospho-ablative mutations (S/A) at the group 1 cluster (e.g., S40, S53, S271, S314, and S315) reduced PDE activity relative to WT or phospho-mimetic (S>D) residues at these sites (Figure 5A). These data suggest that phosphorylation of PDE2 at select residues in the N terminus activates cAMP hydrolysis, whereas dephosphorylation of these residues reduces activity.

To further address the consequence of PDE2 phosphorylation, rPDE2 phospho-mutations from group 1 that resulted in differential activity *in vitro* were expressed in parasites to determine their impact on egress. GCaMP6f was introduced into the *HXGprt* locus of the PDE2-mAID-3HA line to monitor Ca²⁺ while simultaneously regulating the expression of PDE2 (Figures S6A and S6B). Knockdown of PDE2 did not alter the expression GCaMP as determined by western blot analysis and IFA (Figures 6C and 6D). Different versions of C-terminal TY-tagged PDE2 were then introduced into the *UPRT* locus to generate complementation lines that expressed WT, catalytically dead, or phospho-mutant (phospho-mimetic or -ablative mutations in group 1) forms of PDE2 (Figures S5C and S5D). In the constructed merodiploid lines, PDE2-mAID-3HA was degradable by IAA treatment, while the expression of the complemented copies of PDE2 was similar based on western blot analysis and IFA (Figures S5E and S5F).

To determine whether the phosphorylation status of PDE2 impacts egress, we degraded PDE2-mAID-3HA by adding IAA, leaving only the complemented copy of PDE2, and then

Figure 4. Analysis of phosphorylation of PDE2 by PKAc1

- (A) Phosphorylation of PDE2 by PKAc1 following co-expression in *E. coli*. The catalytic domain of PDE2 (PDE2_{CAT}) was co-expressed with PKAc1 (WT or K65H point mutant), affinity purified, and with and without lambda protein phosphatase (PP). Protein samples were evaluated on SDS-PAGE gels supplemented ± Phos-tag using Coomassie brilliant blue (CBB) staining. Representative gel from at least three independent experiments is shown.³²
- (B) Phosphosites of PDE2 identified by mass spectrometry mapped on a predicted Swiss homology model of the PDE2_{CAT}. Phosphorylated residues are labeled in green, and enriched phosphorylated residues are denoted in purple.
- (C) Primary sequence and comparison of PDE2_{CAT} phosphosites identified in here vs. previously.³²
- (D) Immunoprecipitation (IP) of PDE2 from ME49 parasites co-expressing Tir1 PKAc1-mAID-3HA and PDE2-2Strep treated with IAA (500 μM) or diluent (0.1% ethanol). Input and IP samples were analyzed using α-strep and α-HA western blots detected with IR dye-conjugated secondary antibodies. A representative blot from at least three independent experiments is shown. See also Figures S3A and S3B.
- (E) Volcano plot of PDE2 phosphosites from ME49 parasites co-expressing PKAc1-mAID-3HA and PDE2-2Strep treated with IAA (500 μM) or diluent (0.1% ethanol) determined by MaxQuant analysis of mass spectrometry data (*N* = 4). Fold change (x axis) is plotted against the false discovery rate (FDR). Each dot represents a differentially phosphorylated residue, and significantly downregulated residues are labeled and denoted in red. See also Figure S3C.



(legend on next page)

stimulated egress using zaprinast, a PDE inhibitor that elevates cGMP and, thus, activates PKG^{49,50} (Figures 5Ci–5Civ). As expected, complementation with the WT PDE2 restored egress in IAA-treated parasites (Figure 5Ci), while parasites complemented with the catalytically dead enzyme (CAT. dead) form failed to egress in IAA-treated cells stimulated with zaprinast (Figure 5Cii). Parasites expressing the phospho-mimetic form in group 1 sites (i.e., S>D) alone (+IAA) exhibited egress levels that were similar to WT (Figure 5Ciii). In contrast, expression of the phospho-ablative form (i.e., S/A) of PDE2 (+IAA) significantly reduced egress in IAA-treated cells stimulated with zaprinast (Figure 5Civ). Taken together, these results indicate that the phosphorylation of residues in group 1 is required for the full activity of PDE2, which degrades cAMP, thereby suppressing PKAc1 and allowing egress.

PKAc1 targets processes between GC and Ca²⁺ signaling to suppress parasite egress

Our findings are consistent with a negative feedback loop in which PKAc1 phosphorylates PDE2 to activate it, resulting in the degradation of cAMP and eventual shutdown of PKAc1. When this loop is artificially disrupted by degradation of PDE2 late in infection, parasites are reluctant to egress due to the overactivity of PKAc1. This manipulation allowed us to further dissect the point at which PKAc1 exerts its negative feedback on the PKG pathway needed for egress. To do so, we knocked down PDE2-mAID-3HA by adding IAA and then stimulated egress and Ca²⁺ signaling using zaprinast (a PDE inhibitor) or ionomycin (calcium ionophore) (Figure 6A). PDE2-depleted parasites exhibited a significant reduction in egress, as ~80% vacuoles remained intact in comparison to WT parasites (mock) when stimulated with zaprinast (Figure 6B). Moreover, Ca²⁺ signaling in PDE2-depleted parasites was suppressed, consistent with its integral role in parasite egress (Figure 5C). We also probed the response to ionomycin, which acts to release intracellular calcium from the endoplasmic reticulum (ER) and thus is downstream of zaprinast. Treating PDE2-depleted parasites with ionomycin led to elevated Ca²⁺ (Figure 6E), and somewhat surprisingly, this also led to egress at levels comparable to the WT (Figure 6D). These findings indicate that excessive intracellular Ca²⁺ concentrations overcome the block in egress that results from the loss of PDE2. Finally, to confirm that activated PKAc1 blocks egress in PDE2-depleted parasites, the PKA inhibitor H89^{32,51} was used to inhibit PKAc1 prior to zaprinast treatment (Figure 6A). Treatment with H89 partially rescued egress in parasites depleted of PDE2 and stimulated with zaprinast in a dose-

dependent manner (Figure 6E). Treatment with 5 μM H89 partially rescued egress, reaching levels (IAA and H89) that were significantly above untreated levels (IAA) but below WT levels (mock) (Figure 6F). In addition, the inactivation of PKAc1 by H89 also partially rescued calcium signaling in PDE2-depleted parasites (Figure 6G). Altogether, these data indicate that PKAc1 inhibits egress by targeting processes downstream of cGMP production and upstream of Ca²⁺ signaling, respectively (Figure 6H).

DISCUSSION

Previous studies have shown that PKG promotes motility, invasion, and egress, while PKAc1 acts to suppress this pathway, although how this feedback system is regulated was unclear. To pinpoint the role of PKAc1, we used the auxin-induced degron to demonstrate that the conditional knockdown of PKAc1 has no effect in late-stage infection but promotes premature egress after re-invasion, consistent with a temporal role in suppressing PKG and calcium-dependent motility. Among the substrates of PKAc1, the phosphorylation of PDE2 at key residues in the N terminus activates its hydrolysis of cAMP. Thus activated, PDE2 serves as a negative feedback loop by consuming cAMP to downregulate PKAc1. Consistent with this model, conditional degradation of PDE2 in late-stage infection impairs natural and zaprinast-stimulated egress. Surprisingly, this block can be overcome by stimulation with ionomycin, implying that the key substrates of PKAc1 that regulate the egress pathway lie between GC and calcium release. Our studies reveal that PKAc1 is governed by a negative feedback loop that rapidly suppresses the PKG pathway after invasion and allows for quiescent intracellular development.

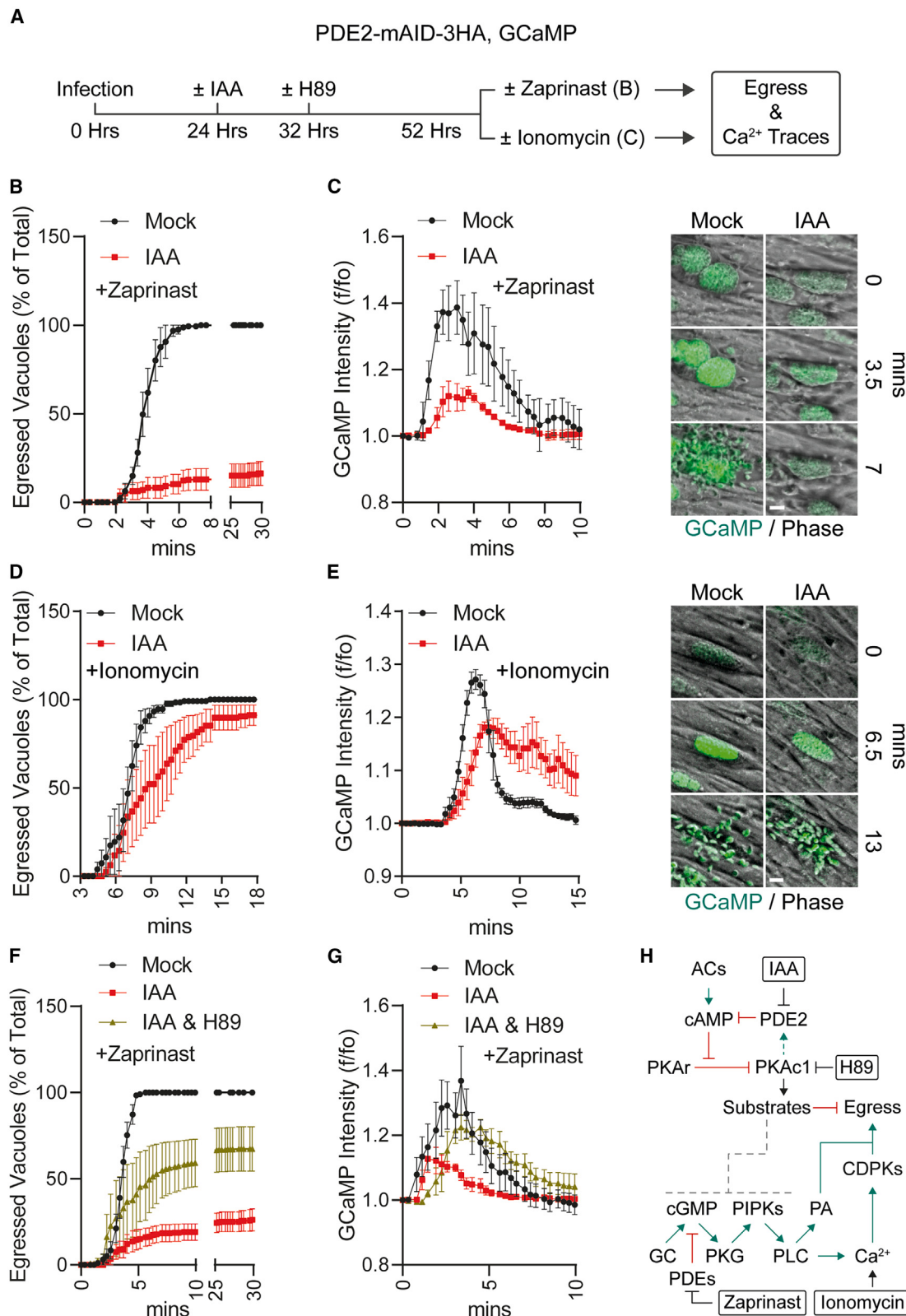
Previous studies using transcriptional downregulation of PKAc1 or stabilization of a dominant-negative PKAr form that does not bind cAMP revealed that inactivation of PKAc1 leads to restless invasion that results from the failure of newly invaded tachyzoites to establish an intracellular niche.^{32,33} Here, we took advantage of the rapid AID protein degradation system to show that when PKAc1-depleted tachyzoites infect new cells, they fail to suppress calcium oscillations and exhibit restless egress, while the loss of PKAc1 in late-stage vacuoles has no effect on natural egress. A slightly different conclusion was reached by a previous study that found that at a high multiplicity of infection (MOI), late-stage vacuoles depleted of PKAc1 by transcriptional repression undergo early egress.³² However, at a high MOI, some vacuoles will lyse due to mechanical failure, releasing

Figure 5. Phosphorylation of PDE2 controls enzymatic activity and parasite egress

(A) Recombinant PDE2-Strep purified from HEK293T cells was tested for activity using cAMP substrate at 30°C for 3 h and 40 min. Mean RLU ± SEM from at least six independent experiments for WT, CAT. dead, and group 1 phospho-mimetic (S>D or T>E) and phospho-ablative (S/T>A), and at least three independent experiments for group 2 and 3 phospho-mimetic (S>D or T>E) and phospho-ablative (S/T>A) are shown. Unpaired Student's t test (WT vs. H1944A and H1945A) and two-way ANOVA (phospho-mimetic vs. -ablative) (*p < 0.05). See also Figures S4A and S4B.

(B) Schematic representation of PDE2-mAID-3HA, GCaMP, cPDE2-2TY (X) parasites, where "X" stands for one of the clustered templates defined below. See also Figures S4C–S4F.

(Ci–Civ) Living imaging of PDE2-mAID-3HA, GCaMP parasites expressing cPDE2-2TY WT (i); H1944A and D1945A (ii); S40D, S53D, S271D, S314D, and S315D (iii); and S40A, S53A, S271A, S314A, and S315A (iv). Infected HFF cells were treated with IAA (500 μM) or diluent (0.1% ethanol) at 24 hpi prior to stimulation with DMSO or zaprinast (250 μM) at 50 hpi. Representative time-lapse images of IAA- or ethanol-treated parasites following stimulation with zaprinast are shown. Egressed vacuoles were calculated as a percentage of lysed vacuoles vs. total number of vacuoles as a function of time. Means ± SE from at least three independent experiments are shown.



(legend on next page)

parasites that invade nearby cells but then rapidly egress, in turn triggering egress of previously established vacuoles. By using a low MOI, our study identified a temporal role for PKAc1 in suppressing calcium signaling and preventing egress immediately after invasion, while it is dispensable at later stages.

A previous study examining PKAc1-dependent targets identified PDE2 as having several residues with decreased phosphorylation in the absence of PKAc1.³² Because PDE2 contains a conserved GAF domain (found in cGMP regulated phosphodiesterases), which is typical of enzymes that degrade cGMP,⁵² it was proposed that PKAc1 may downregulate the PKG pathway by activating PDE2 to consume cGMP.³² However, PDE2 from *T. gondii* lysates showed almost exclusive activity against cAMP, consistent with other recent reports using purified recombinant enzymes.^{23,43,44} GAF domains have also been shown to modulate the function of PDEs,⁵² and thus, it is possible that the binding of cGMP by PDE2 modulates its activity against cAMP. Additionally, the observation that PDE2 is a target of PKA suggests that the phosphorylation of PDE2 activates the enzyme to consume cAMP. Several lines of evidence support this model, including that the degradation of both PKAc1 or PDE2 resulted in elevated cAMP in the parasite and that the loss of PKAc1 phosphorylate sites in PDE2 diminished its activity, as discussed further below. Interestingly, the loss of PDE2 also led to a slight decrease in cGMP, which is likely an indirect effect. To further probe the role of PDE2, we generated a conditional knockdown line and showed that it exhibits a dramatic loss of growth *in vitro*. Similar phenotypes were reported by others using the auxin degron system to conditionally repress PDE2 in the type I RH strain.^{43,45} Our studies further defined the role of PDE2 in late-stage infection by showing that its loss results in decreased natural egress and resistance to stimulation by zaprinast, which would normally raise cGMP levels and activate the PKG pathway.^{14,15} These findings are consistent with PDE2 serving as a negative feedback loop to suppress PKAc1, which remains active when PDE2 is depleted, thus preventing activation of the PKG pathway.

By examining PKAc1-dependent phosphorylation sites in PDE2, we identified a cluster of S/T resides in the N terminus that were important for function and a phosphorylation motif for PKAc1 that loosely resembles the conical PKA phosphorylation motif of RRXS/TY.⁵³ Altering these resides to aspartic acid, to mimic the negative charge of phosphorylation, had no effect on the hydrolysis of cAMP by PDE2, consistent with their phosphorylation being important for activity. In contrast, altering these residues to alanine to prevent phosphorylation both decreased cAMP hydrolysis by purified PDE2 *in vitro*

and led to impaired rescue of a conditional knockdown of PDE2 in the parasite. These findings are consistent with PKAc1 phosphorylation of the N terminus of PDE2 resulting in activation, similar to the regulation of PDEs in other systems.^{47,54} The cluster of residues in the N terminus of PDE2 lies outside the active site and, therefore, must act allosterically or through long-range interactions. N-terminal regions in mammalian and yeast PDEs are known to contain various domains that impart regulation on the catalytic domain, including cyclic nucleotide binding sites, phosphorylation sites, and autoinhibitory regions.^{47,54}

Combined with prior studies, our findings provide a holistic model for how the lytic cycle of *T. gondii* tachyzoites is regulated (Figure 7). Prior to invasion, the PKG pathway is active to support microneme secretion, motility, and invasion. The model predicts that PKAc1 should be off at this stage, but it needs to be rapidly activated upon entry to prevent premature egress (Figure 7). Hence, cAMP levels likely rise rapidly after invasion, a process mediated primarily by AC α 3 (Figure 7), although the partial phenotype of the knockout suggests the other ACs also contribute. After entry, the model predicts that PKAc1 shuts down the PKG pathway to prevent premature egress (Figure 7). Our findings implicate PKAc1 targets between GC and the calcium release step in this process (Figure 7). Additionally, PKAc1 also phosphorylates PDE2 to activate it, thus consuming cAMP and resulting in PKAc1 shutdown (Figure 7). Late in the cycle, PKAc1 remains off, while the PKG pathway again becomes active. Reactivation of the PKG pathway could result from a phosphatase that removes inhibitory phosphorylation events imparted by PKAc1. However, it is also possible that resetting the activation state is accomplished by protein turnover during replication, as newly synthesized proteins would lack the inhibitory modifications. Late in the cycle, there are also changes that activate the PKG pathway, including the accumulation of phosphatidic acid⁹ and a drop in the vacuole pH,⁵⁵ and additionally, both PKG and PKA are under the control of SPARK.⁵⁶ Collectively, these additional inputs may form a time-dependent, feedforward network that turns the PKG pathway back on once a critical threshold has been reached for activation.

There are many examples of positive and negative feedback loops in biology that govern complex signaling pathways.⁵⁷ Based on shared targets and common outputs, it has previously been proposed that PKG, CDPK1, and CDPK3 form a positive activating loop to upregulate a common pathway needed for motility during invasion and egress.²³ Such positive loops can both accelerate the timing and increase the

Figure 6. PDE2 regulates egress by controlling PKAc1 activity

(A) Schematic of the experimental design.

(B-E) Live imaging of zaprinast- or ionomycin-stimulated egress and GCaMP fluorescence of ME49 parasites expressing Tir1 PDE2-mAID-3HA and GCaMP. Infected HFF cells were treated with IAA (500 μ M) or diluent (0.1% ethanol) at 24 hpi, stimulated with DMSO, 250 μ M zaprinast (B and C), or 1 μ M ionomycin (D and E), and assessed for egress (B and C) or GCaMP fluorescence (C and E) by live imaging at 52 hpi. Insets show time-lapse images of IAA- or ethanol-treated parasites in the presence of zaprinast (C) or 1 μ M ionomycin (E). DMSO was used in the mock control. Scale bar: 5 μ m. See also Figures S5A-S5D.

(F and G) Egress and calcium profiles of IAA- (500 μ M) or diluent- (0.1% ethanol) treated parasites treated with H89. IAA- or ethanol-treated PDE2-mAID-3HA, GCaMP parasite-infected cells were incubated with 5 μ M H89 prior to live imaging in the presence of 250 μ M zaprinast. See also Figure S5E. For time-course egress assays, egressed vacuoles were calculated as a percentage of lysed vacuoles vs. total number of vacuoles as a function of time. Means \pm SE from at least 3 independent experiments are shown.

(H) Schematic depicting PKG and PKAc1 pathways regulating egress.

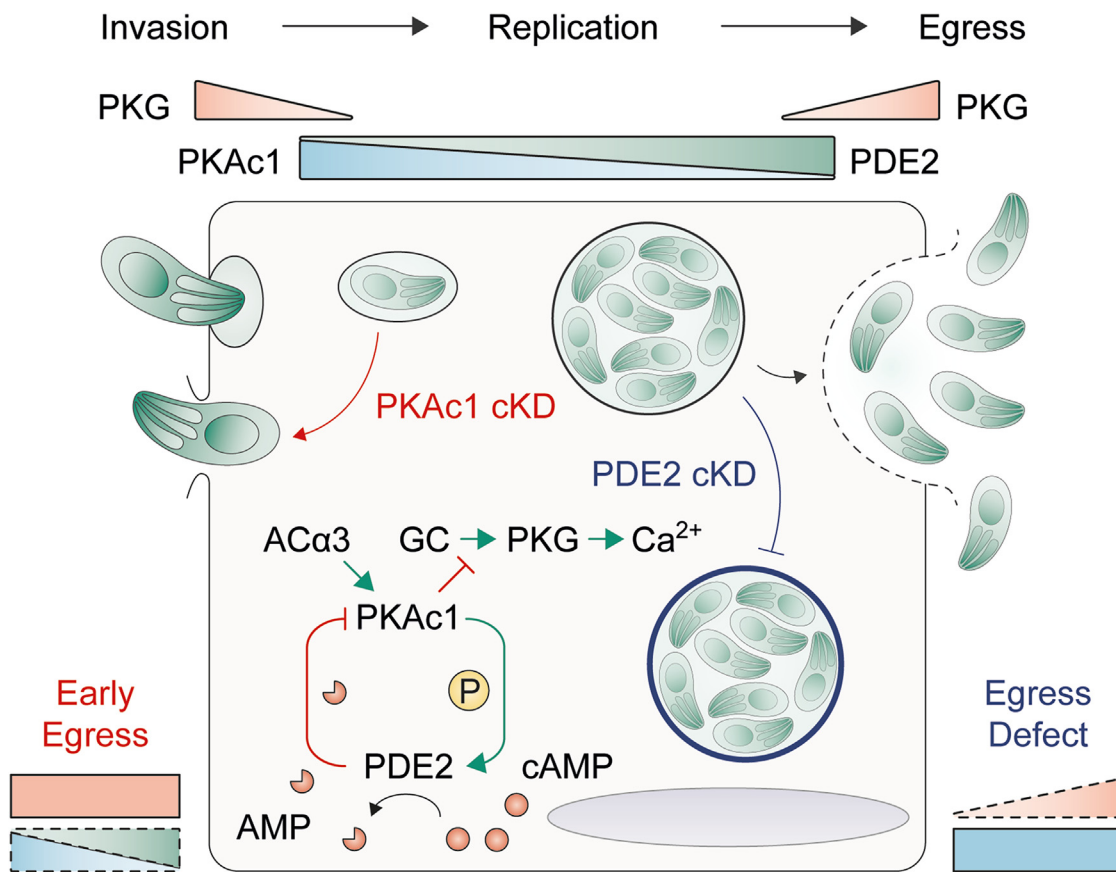


Figure 7. Model for control of lytic cycle

During extracellular motility and invasion, the PKG pathway is activated. Shortly after invasion, adenylate cyclases (ACs; primarily AC α 3) are activated to generate cAMP, thus activating protein kinase A c1 (PKAc1). PKAc1 shuts down the PKG pathway by phosphorylating substrates between guanylate cyclase and calcium release, thus preventing premature egress. PKAc1 also phosphorylates phosphodiesterase 2 (PDE2) to activate cAMP hydrolysis. This negative feedback loop is predicted to result in the transient activation of PKAc1. Support for this model is provided by the conditional degradation of PKAc1, which leads to premature egress (red arrow) when the PKG pathway is not inhibited. Additionally, conditional repression of PDE2 blocks egress (purple inhibition line) due to a failure to downregulate PKAc1, which in turn suppresses PKG, which is needed at the end of the cycle. Triangles represent increasing or decreasing activity, whereas rectangles denote constant activity. Dashed lines indicate loss of activity due to conditional knockout. PKG, PKAc1, and PDE2 activities are represented by orange, blue, and green colors, respectively.

amplitude of the response and are advantageous when a full-on response is optimal.⁵⁷ By contrast, negative feedback loops are advantageous in situations where graded or limited outputs are desirable.⁵⁷ The interaction of PKAc1 and PDE2 is a specialized example of a negative feedback loop where the initial action is to activate (i.e., the action of PKAc1 on PDE2) while the second step is to inhibit the original input (i.e., the action of PDE2 action on PKAc1), a process that is predicted to lead to the transient activation of PKAc1.⁵⁷ Considering evidence that PKAc1 also counteracts PKG, it is noteworthy that the PKG/CDPK1 pathway acts as a bistable switch, exhibiting both rapid activation and rapid shutoff. The lytic cycle of *T. gondii* tachyzoite growth is controlled by a complex feedforward pathway to activate a PKG/CDPK-dependent pathway that controls motility, invasion, and egress. PKAc1 counteracts this pathway by rapidly returning it to its ground state after invasion. In turn, PKAc1 is regulated by a negative feedback loop, ensuring that it is transiently activated after invasion. Collectively, these feedforward and feedback networks allow the parasite to respond to environmental signals to rapidly activate motility when the need arises to exit one cell and enter another, interspersed by longer periods of quiescent intracellular growth.

siently activated after invasion. Collectively, these feedforward and feedback networks allow the parasite to respond to environmental signals to rapidly activate motility when the need arises to exit one cell and enter another, interspersed by longer periods of quiescent intracellular growth.

Limitations of the study

Our studies implicate the phosphorylation of key residues in the N terminus of PDE in activating its PDE activity. How the phosphorylation of residues in the N-terminal region might impact the activity of the catalytic domain is uncertain given the unstructured nature of this region. Our findings also imply that the phosphorylation of key targets in the PKG pathway by PKAc1 returns the system to its off state. Testing this model further would benefit from time-dependent analysis of PKAc1-dependent phosphorylation targets immediately after invasion, when its activity is predicted to be maximum. Additionally, further analysis of PKAc1 substrates using synthetic

peptide arrays could potentially better define its substrate specificity, which could be useful in the search for additional substrates in the parasite proteome.

RESOURCE AVAILABILITY

Lead contact

Further information and requests for resources and reagents should be directed to and will be fulfilled by the lead contact, L. David Sibley (sibley@wustl.edu).

Materials availability

All materials generated in this study are available under standard material transfer agreements from Washington University.

Data and code availability

- All data associated with the study are found in the figures and accompanying [supplemental information](#).
- No new code was generated in this study.
- Any additional information required to reanalyze the data reported in this paper is available from the lead contact upon request.

ACKNOWLEDGMENTS

MS analyses were performed by the Mass Spectrometry Technology Access Center at McDonnell Genome Institute (MTAC@MGI) at Washington University School of Medicine. We thank Jenn Barks for technical assistance with cell cultures and members of the Sibley lab for helpful advice. We are also grateful to Kami Kim for advice and discussion. This work was supported by a grant from NIH (AI162749).

AUTHOR CONTRIBUTIONS

Conceptualization, J.E.C., Y.F., and L.D.S.; data curation, J.E.C. and Y.F.; formal analysis, J.E.C. and Y.F.; investigation, J.E.C. and Y.F.; methodology, J.E.C. and Y.F.; visualization, J.E.C.; writing – original draft, J.E.C. and L.D.S.; writing – review & editing, L.D.S.; supervision, L.D.S.; project administration, L.D.S.

DECLARATION OF INTERESTS

The authors declare no competing interests.

STAR★METHODS

Detailed methods are provided in the online version of this paper and include the following:

- [KEY RESOURCES TABLE](#)
- [EXPERIMENTAL MODEL AND STUDY PARTICIPANT DETAILS](#)
 - Parasite and host cell culture
- [METHOD DETAILS](#)
 - Plasmid construction
 - Generation of transgenic parasites
 - Western blotting
 - If microscopy
 - Plaque formation assay
 - Purification of recombinant PDE2 (rPDE2)
 - PDE assays
 - cAMP and cGMP ELISA assays
 - PhosTag gels
 - Identification of PDE2 phosphosites
 - Egress assays
- [QUANTIFICATION AND STATISTICAL ANALYSIS](#)
 - Statistics

SUPPLEMENTAL INFORMATION

Supplemental information can be found online at <https://doi.org/10.1016/j.celrep.2025.115260>.

Received: August 22, 2024

Revised: November 27, 2024

Accepted: January 13, 2025

Published: February 3, 2025

REFERENCES

1. Dubey, J.P. (2010). *Toxoplasmosis of Animals and Humans* (CRC Press).
2. Sibley, L.D. (2004). Invasion strategies of intracellular parasites. *Science* 304, 248–253.
3. Frenal, K., Dubremetz, J.F., Lebrun, M., and Soldati-Favre, D. (2017). Gliding motility powers invasion and egress in Apicomplexa. *Nat. Rev. Microbiol.* 15, 645–660. <https://doi.org/10.1038/nrmicro.2017.86>.
4. Blader, I.J., Coleman, B.I., Chen, C.T., and Gubbels, M.J. (2015). Lytic Cycle of *Toxoplasma gondii*: 15 Years Later. *Annu. Rev. Microbiol.* 69, 463–485. <https://doi.org/10.1146/annurev-micro-091014-104100>.
5. Wiersma, H.I., Galuska, S.E., Tomley, F.M., Sibley, L.D., Liberator, P.A., and Donald, R.G.K. (2004). A role for coccidian cGMP-dependent protein kinase in motility and invasion. *Int. J. Parasitol.* 34, 369–380.
6. Brown, K.M., Long, S., and Sibley, L.D. (2017). Plasma membrane association by N-acylation governs PKG function in *Toxoplasma gondii*. *mBio* 8, e00375-17.
7. Billker, O., Lourido, S., and Sibley, L.D. (2009). Calcium-dependent signaling and kinases in apicomplexan parasites. *Cell Host Microbe* 5, 612–622.
8. Brown, K.M., and Sibley, L.D. (2018). Essential cGMP Signaling in Toxoplasma Is Initiated by a Hybrid P-Type ATPase-Guanylate Cyclase. *Cell Host Microbe* 24, 804–816. <https://doi.org/10.1016/j.chom.2018.10.015>.
9. Bisio, H., Lunghi, M., Brochet, M., and Soldati-Favre, D. (2019). Phosphatidic acid governs natural egress in *Toxoplasma gondii* via a guanylate cyclase receptor platform. *Nat. Microbiol.* 4, 420–428. <https://doi.org/10.1038/s41564-018-0339-8>.
10. Yang, L., Ubaldi, A.D., Seizova, S., Wilde, M.L., Coffey, M.J., Katris, N.J., Yamaryo-Botté, Y., Kocan, M., Bathgate, R.A.D., Stewart, R.J., et al. (2019). An apically located hybrid guanylate cyclase-ATPase is critical for the initiation of Ca(2+) signaling and motility in *Toxoplasma gondii*. *J. Biol. Chem.* 294, 8959–8972. <https://doi.org/10.1074/jbc.RA118.005491>.
11. Lovett, J.L., and Sibley, L.D. (2003). Intracellular calcium stores in *Toxoplasma gondii* govern invasion of host cells. *J. Cell Sci.* 116, 3009–3016.
12. Pace, D.A., McKnight, C.A., Liu, J., Jimenez, V., and Moreno, S.N.J. (2014). Calcium entry in *Toxoplasma gondii* and its enhancing effect of invasion-linked traits. *J. Biol. Chem.* 289, 19637–19647, jbc.M114.565390 [pii]. <https://doi.org/10.1074/jbc.M114.565390>.
13. Alam, M.M., Solyakov, L., Bottrill, A.R., Flueck, C., Siddiqui, F.A., Singh, S., Mistry, S., Viskaduraki, M., Lee, K., Hopp, C.S., et al. (2015). Phosphoproteomics reveals malaria parasite Protein Kinase G as a signalling hub regulating egress and invasion. *Nat. Commun.* 6, 7285. <https://doi.org/10.1038/ncomms8285>.
14. Sidik, S.M., Hortua Triana, M.A., Paul, A.S., El Bakkouri, M., Hackett, C.G., Tran, F., Westwood, N.J., Hui, R., Zuercher, W.J., Duraisingham, M.T., et al. (2016). Using a Genetically Encoded Sensor to Identify Inhibitors of *Toxoplasma gondii* Ca2+ Signaling. *J. Biol. Chem.* 291, 9566–9580. <https://doi.org/10.1074/jbc.M115.703546>.
15. Brown, K.M., Lourido, S., and Sibley, L.D. (2016). Serum Albumin Stimulates Protein Kinase G-dependent Microneme Secretion in *Toxoplasma gondii*. *J. Biol. Chem.* 291, 9554–9565. <https://doi.org/10.1074/jbc.M115.700518>.
16. Smith, T.A., Lopez-Perez, G.S., Herneisen, A.L., Shortt, E., and Lourido, S. (2022). Screening the *Toxoplasma* genome with high-throughput tagging

- identifies a regulator of invasion and egress. *Nat. Microbiol.* 7, 868–881. <https://doi.org/10.1038/s41564-022-01104-0>.
17. Lourido, S., Shuman, J., Zhang, C., Shokat, K.M., Hui, R., and Sibley, L.D. (2010). Calcium-dependent protein kinase 1 is an essential regulator of exocytosis in *Toxoplasma*. *Nature* 465, 359–362.
 18. Wernimont, A.K., Artz, J.D., Finerty, P., Lin, Y.H., Amani, M., Allali-Hassani, A., senisterra, G., Vedadi, M., Tempel, W., Mackenzie, F., et al. (2010). Structures of apicomplexan calcium-dependent protein kinases reveal mechanism of activation by calcium. *Nat. Struct. Mol. Biol.* 17, 596–601.
 19. Shortt, E., Hackett, C.G., Stadler, R.V., Kent, R.S., Herneisen, A.L., Ward, G.E., and Lourido, S. (2023). CDPK2A and CDPK1 form a signaling module upstream of *Toxoplasma* motility. *mBio* 14, e0135823. <https://doi.org/10.1128/mBio.01358-23>.
 20. Lourido, S., Tang, K., and Sibley, L.D. (2012). Distinct signalling pathways control *Toxoplasma* egress and host-cell invasion. *EMBO J.* 31, 4524–4534.
 21. McCoy, J.M., Whitehead, L., van Dooren, G.G., and Tonkin, C.J. (2012). TgCDPK3 regulates calcium-dependent egress of *Toxoplasma gondii* from host cells. *PLoS Pathog.* 8, e1003066, [pii]. <https://doi.org/10.1371/journal.ppat.1003066> PPATHOGENS-D-12-01390.
 22. Garrison, E., Treeck, M., Ehret, E., Butz, H., Garbuza, T., Oswald, B.P., Settles, M., Boothroyd, J., and Arrizabalaga, G. (2012). A forward genetic screen reveals that calcium-dependent protein kinase 3 regulates egress in *Toxoplasma*. *PLoS Pathog.* 8, e1003049, [pii]. <https://doi.org/10.1371/journal.ppat.1003049> PPATHOGENS-D-12-01362.
 23. Nofal, S.D., Dominicus, C., Broncel, M., Katris, N.J., Flynn, H.R., Arrizabalaga, G., Botté, C.Y., Invergo, B.M., and Treeck, M. (2022). A positive feedback loop mediates crosstalk between calcium, cyclic nucleotide and lipid signalling in calcium-induced *Toxoplasma gondii* egress. *PLoS Pathog.* 18, e1010901. <https://doi.org/10.1371/journal.ppat.1010901>.
 24. Farrell, A., Thirugnanam, S., Lorestani, A., Dvorin, J.D., Eidell, K.P., Ferguson, D.J.P., Anderson-White, B.R., Duraisingham, M.T., Marth, G.T., and Gubbels, M.J. (2012). A DOC2 protein identified by mutational profiling is essential for apicomplexan parasite exocytosis. *Science* 335, 218–221, 335/6065/218 [pii]. <https://doi.org/10.1126/science.1210829>.
 25. Coleman, B.I., Saha, S., Sato, S., Engelberg, K., Ferguson, D.J.P., Coppen, I., Lodoen, M.B., and Gubbels, M.J. (2018). A Member of the Ferlin Calcium Sensor Family Is Essential for *Toxoplasma gondii* Rhoptry Secretion. *mBio* 9, e01510-18. <https://doi.org/10.1128/mBio.01510-18>.
 26. Wetzel, D.M., Chen, L.A., Ruiz, F.A., Moreno, S.N.J., and Sibley, L.D. (2004). Calcium-mediated protein secretion potentiates motility by *Toxoplasma gondii*. *J. Cell Sci.* 117, 5739–5748.
 27. Vieira, M.C., and Moreno, S.N. (2000). Mobilization of intracellular calcium upon attachment of *Toxoplasma gondii* tachyzoites to human fibroblasts is required for invasion. *Mol. Biochem. Parasitol.* 106, 157–162.
 28. Borges-Pereira, L., Budu, A., McKnight, C.A., Moore, C.A., Vella, S.A., Hortua Triana, M.A., Liu, J., Garcia, C.R.S., Pace, D.A., and Moreno, S.N.J. (2015). Calcium Signaling throughout the *Toxoplasma gondii* Lytic Cycle: A STUDY USING GENETICALLY ENCODED CALCIUM INDICATORS. *J. Biol. Chem.* 290, 26914–26926. <https://doi.org/10.1074/jbc.M115.652511>.
 29. Sugi, T., Ma, Y.F., Tomita, T., Murakoshi, F., Eaton, M.S., Yakubu, R., Han, B., Tu, V., Kato, K., Kawazu, S.I., et al. (2016). *Toxoplasma gondii* Cyclic AMP-Dependent Protein Kinase Subunit 3 Is Involved in the Switch from Tachyzoite to Bradyzoite Development. *mBio* 7, e00755-16. <https://doi.org/10.1128/mBio.00755-16>.
 30. Hehl, A.B., Basso, W.U., Lippuner, C., Ramakrishnan, C., Okoniewski, M., Walker, R.A., Grigg, M.E., Smith, N.C., and Deplazes, P. (2015). Asexual expansion of *Toxoplasma gondii* merozoites is distinct from tachyzoites and entails expression of non-overlapping gene families to attach, invade, and replicate within feline enterocytes. *BMC Genom.* 16, 66. <https://doi.org/10.1186/s12864-015-1225-x>.
 31. Behnke, M.S., Zhang, T.P., Dubey, J.P., and Sibley, L.D. (2014). *Toxoplasma gondii* merozoite gene expression analysis with comparison to the life cycle discloses a unique expression state during enteric development. *BMC Genom.* 15, 350, [pii]. <https://doi.org/10.1186/1471-2164-15-350>.
 32. Jia, Y., Marq, J.B., Bisio, H., Jacot, D., Mueller, C., Yu, L., Choudhary, J., Brochet, M., and Soldati-Favre, D. (2017). Crosstalk between PKA and PKG controls pH-dependent host cell egress of *Toxoplasma gondii*. *EMBO J.* 36, 3250–3267. <https://doi.org/10.15252/embj.201796794>.
 33. Ubaldi, A.D., Wilde, M.L., McRae, E.A., Stewart, R.J., Dagley, L.F., Yang, L., Katris, N.J., Hapuarachchi, S.V., Coffey, M.J., Lehane, A.M., et al. (2018). Protein kinase A negatively regulates Ca²⁺ signalling in *Toxoplasma gondii*. *PLoS Biol.* 16, e2005642. <https://doi.org/10.1371/journal.pbio.2005642>.
 34. Brown, K.M., Long, S., and Sibley, L.D. (2018). Conditional Knockdown of Proteins Using Auxin-inducible Degron (AID) Fusions in *Toxoplasma gondii*. *Bio. Protoc.* 8, e2728. <https://doi.org/10.21769/BioProtoc.2728>.
 35. Brown, K.M., Long, S., and Sibley, L.D. (2017). Plasma Membrane Association by N-Acylation Governs PKG Function in *Toxoplasma gondii*. *mBio* 8, e00375-17. <https://doi.org/10.1128/mBio.00375-17>.
 36. Taylor, S.S., Wu, J., Bruystens, J.G.H., Del Rio, J.C., Lu, T.W., Kornev, A.P., and Ten Eyck, L.F. (2021). From structure to the dynamic regulation of a molecular switch: A journey over 3 decades. *J. Biol. Chem.* 296, 100746. <https://doi.org/10.1016/j.jbc.2021.100746>.
 37. Mueller, C., Samoo, A., Hammoudi, P.M., Klages, N., Kallio, J.P., Kursula, I., and Soldati-Favre, D. (2016). Structural and functional dissection of *Toxoplasma gondii* armadillo repeats only protein. *J. Cell Sci.* 129, 1031–1045. <https://doi.org/10.1242/jcs.177386>.
 38. Schultz, J.E., Kanchan, K., and Ziegler, M. (2015). Intraprotein signal transduction by HAMP domains: a balancing act. *Int. J. Med. Microbiol.* 305, 243–251. <https://doi.org/10.1016/j.ijmm.2014.12.007>.
 39. Cerveny, L., Straskova, A., Dankova, V., Hartlova, A., Ceckova, M., Staud, F., and Stulik, J. (2013). Tetrastricopeptide repeat motifs in the world of bacterial pathogens: role in virulence mechanisms. *Infect. Immun.* 81, 629–635. <https://doi.org/10.1128/IAI.01035-12>.
 40. Stuffle, E.C., Johnson, M.S., and Watts, K.J. (2021). PAS domains in bacterial signal transduction. *Curr. Opin. Microbiol.* 61, 8–15. <https://doi.org/10.1016/j.mib.2021.01.004>.
 41. Zimmermann, L., Stephens, A., Nam, S.Z., Rau, D., Kübler, J., Lozajic, M., Gabler, F., Söding, J., Lupas, A.N., and Alva, V. (2018). A Completely Re-implemented MPI Bioinformatics Toolkit with a New HHpred Server at its Core. *J. Mol. Biol.* 430, 2237–2243. <https://doi.org/10.1016/j.jmb.2017.12.007>.
 42. Gabler, F., Nam, S.Z., Till, S., Mirdita, M., Steinegger, M., Söding, J., Lupas, A.N., and Alva, V. (2020). Protein Sequence Analysis Using the MPI Bioinformatics Toolkit. *Curr. Protoc. Bioinformatics* 72, e108. <https://doi.org/10.1002/cpbi.108>.
 43. Moss, W.J., Patterson, C.E., Jochmans, A.K., and Brown, K.M. (2022). Functional Analysis of the Expanded Phosphodiesterase Gene Family in *Toxoplasma gondii* Tachyzoites. *mSphere* 7, e0079321. <https://doi.org/10.1128/msphere.00793-21>.
 44. Vo, K.C., Günay-Esiyok, Ö., Liem, N., and Gupta, N. (2020). The protozoan parasite *Toxoplasma gondii* encodes a gamut of phosphodiesterases during its lytic cycle in human cells. *Comput. Struct. Biotechnol. J.* 18, 3861–3876. <https://doi.org/10.1016/j.csbj.2020.11.024>.
 45. Vo, K.C., Ruga, L., Psathaki, O.E., Franzkoch, R., Distler, U., Tenzer, S., Hensel, M., Hegemann, P., and Gupta, N. (2022). Plasticity and therapeutic potential of cAMP and cGMP-specific phosphodiesterases in *Toxoplasma gondii*. *Comput. Struct. Biotechnol. J.* 20, 5775–5789. <https://doi.org/10.1016/j.csbj.2022.09.022>.
 46. Treeck, M., Sanders, J.L., Elias, J.E., and Boothroyd, J.C. (2011). The phosphoproteomes of *Plasmodium falciparum* and *Toxoplasma gondii* reveal unusual adaptations within and beyond the parasites' boundaries.

- Cell Host Microbe 10, 410–419, S1931-3128(11)00288-5 [pii]. <https://doi.org/10.1016/j.chom.2011.09.004>.
47. Keravis, T., and Lugnier, C. (2012). Cyclic nucleotide phosphodiesterase (PDE) isoforms as targets of the intracellular signalling network: benefits of PDE inhibitors in various diseases and perspectives for future therapeutic developments. Br. J. Pharmacol. 165, 1288–1305. <https://doi.org/10.1111/j.1476-5381.2011.01729.x>.
48. Vandamme, J., Castermans, D., and Thevelein, J.M. (2012). Molecular mechanisms of feedback inhibition of protein kinase A on intracellular cAMP accumulation. Cell. Signal. 24, 1610–1618. <https://doi.org/10.1016/j.cellsig.2012.04.001>.
49. Lourido, S., Tang, K., and Sibley, L.D. (2012). Distinct signalling pathways control Toxoplasma egress and host-cell invasion. EMBO J. 31, 4524–4534. <https://doi.org/10.1038/emboj.2012.299>.
50. Howard, B.L., Harvey, K.L., Stewart, R.J., Azevedo, M.F., Crabb, B.S., Jennings, I.G., Sanders, P.R., Manallack, D.T., Thompson, P.E., Tonkin, C.J., and Gilson, P.R. (2015). Identification of potent phosphodiesterase inhibitors that demonstrate cyclic nucleotide-dependent functions in apicomplexan parasites. ACS Chem. Biol. 10, 1145–1154. <https://doi.org/10.1021/cb501004q>.
51. Chijiwa, T., Mishima, A., Hagiwara, M., Sano, M., Hayashi, K., Inoue, T., Naito, K., Toshioka, T., and Hidaka, H. (1990). Inhibition of forskolin-induced neurite outgrowth and protein phosphorylation by a newly synthesized selective inhibitor of cyclic AMP-dependent protein kinase, N-[2-(p-bromocinnamylamino)ethyl]-5-isoquinolinesulfonamide (H-89), of PC12D pheochromocytoma cells. J. Biol. Chem. 265, 5267–5272.
52. Zoragh, R., Corbin, J.D., and Francis, S.H. (2004). Properties and functions of GAF domains in cyclic nucleotide phosphodiesterases and other proteins. Mol. Pharmacol. 65, 267–278. <https://doi.org/10.1124/mol.65.2.267>.
53. Hennrich, M.L., Marino, F., Groenewold, V., Kops, G.J.P.L., Mohammed, S., and Heck, A.J.R. (2013). Universal quantitative kinase assay based on diagonal SCX chromatography and stable isotope dimethyl labeling provides high-definition kinase consensus motifs for PKA and human Mps1. J. Proteome Res. 12, 2214–2224. <https://doi.org/10.1021/pr400074f>.
54. Omori, K., and Kotera, J. (2007). Overview of PDEs and their regulation. Circ. Res. 100, 309–327. <https://doi.org/10.1161/01.RES.0000256354.95791.f1>.
55. Roiko, M.S., Svezhova, N., and Carruthers, V.B. (2014). Acidification Activates Toxoplasma gondii Motility and Egress by Enhancing Protein Secretion and Cytolytic Activity. PLoS Pathog. 10, e1004488. <https://doi.org/10.1371/journal.ppat.1004488>.
56. Herneisen, A.L., Peters, M.L., Smith, T.A., Shortt, E., and Lourido, S. (2024). SPARK Regulates AGC Kinases Central to the Toxoplasma Gondii Asexual Cycle. bioRxiv. <https://doi.org/10.1101/2023.10.30.564746>.
57. Brandman, O., and Meyer, T. (2008). Feedback loops shape cellular signals in space and time. Science 322, 390–395. <https://doi.org/10.1126/science.1160617>.
58. Bastin, P., Bagherzadeh, Z., Matthews, K.R., and Gull, K. (1996). A novel epitope tag system to study protein targeting and organelle biogenesis in *Trypanosoma brucei*. Mol. Biochem. Parasitol. 77, 235–239.
59. Starnes, G.L., Jewett, T.J., Carruthers, V.B., and Sibley, L.D. (2006). Two separate, conserved acidic amino acid domains within the Toxoplasma gondii MIC2 cytoplasmic tail are required for parasite survival. J. Biol. Chem. 281, 30745–30754. <https://doi.org/10.1074/jbc.M606523200>.
60. Aricescu, A.R., Lu, W., and Jones, E.Y. (2006). A time- and cost-efficient system for high-level protein production in mammalian cells. Acta Crystallogr. D Biol. Crystallogr. 62, 1243–1250. <https://doi.org/10.1107/S0907444906029799>.
61. Cox, J., and Mann, M. (2008). MaxQuant enables high peptide identification rates, individualized p.p.b.-range mass accuracies and proteome-wide protein quantification. Nat. Biotechnol. 26, 1367–1372. <https://doi.org/10.1038/nbt.1511>.

STAR★METHODS

KEY RESOURCES TABLE

REAGENT or RESOURCE	SOURCE	IDENTIFIER
Antibodies		
Mouse anti-Ty	A gift from P. Bastin ⁵⁸	mAB Clone BB2
Mouse anti-HA.11	BioLegend	Cat#901501 RRID:AB_2565334
Rabbit anti-HA	Thermo Fisher	Cat#71-5500 RRID:AB_2533988
Rabbit anti-TgAldolase	Sibley lab ⁵⁹	Polyclonal
Mouse anti-Strep	BioLegend	Cat#688202 RRID:AB_2629594
Alexa Fluor 488 Goat anti-mouse IgG (H + L)	Thermo Fisher	Cat#A-11029 RRID:AB_2534088
Alexa Fluor 488 Goat anti-rabbit IgG (H + L)	Thermo Fisher	Cat#A-11008 RRID:AB_143165
Alexa Fluor 568 Goat anti-mouse IgG (H + L)	Thermo Fisher	Cat#A-11031 RRID:AB_144696
Alexa Fluor 568 Goat anti-rabbit IgG (H + L)	Thermo Fisher	Cat#A-11011 RRID:AB_143157
IRDye 800CW Goat anti-mouse IgG (H + L)	LI-COR Biosciences	Cat#925-32210 RRID:AB_2687825
IRDye 800CW Goat anti-rabbit IgG (H + L)	LI-COR Biosciences	Cat#925-32211 RRID:AB_2651127
IRDye 680RD Goat anti-mouse IgG (H + L)	LI-COR Biosciences	Cat#925-68070 RRID:AB_2651128
IRDye 800CW Goat anti-rabbit IgG (H + L)	LI-COR Biosciences	Cat#925-68071 RRID:AB_2721181
Bacterial and virus strains		
NEB5α	New England Biolabs	Cat#C2987I
Rosetta (DE3) Competent Cells	Millipore Sigma	Cat#70954
Chemicals, peptides, and recombinant proteins		
Dulbecco's modified Eagle's medium	Thermo Fisher	Cat#12800
HyClone fetal bovine serum	Thermo Fisher Scientific	Cat#SH30070.03
Gentamicin	Thermo Fisher	Cat# 15710072
L-Glutamine	Millipore Sigma	Cat#G7513
3-indoleacetic acid (IAA/auxin)	Millipore Sigma	Cat#I2886
Bovine serum albumin	Millipore Sigma	Cat#B4287
Ethanol	Parmco-Aaper	Cat#11100020S
Zaprinast	Millipore Sigma	Cat#684500
Ionomycin	Millipore Sigma	Cat#I9657
Crystal violet	Millipore Sigma	Cat#C0775
CellLytic M	Millipore Sigma	Cat#C2978
CellLytic B	Millipore Sigma	Cat#B7310
EcoRI	New England Biolabs	Cat#R0101
NotI	New England Biolabs	Cat#R3189
Q5 polymerase	New England Biolabs	Cat#M0491
Taq polymerase	New England Biolabs	Cat#M0273
Benzonase nuclease	Millipore Sigma	Cat# E1014
Pierce Protease Inhibitor Mini Tablets	Thermo Fisher Scientific	Cat# A32955
PhosSTOP	Millipore Sigma	Cat#4906845001
Lambda Protein Phosphatase	New England Biolabs	Cat# P0753
Strep-Tactin®XT 4Flow® resin	iba-lifesciences	2-5010-002
Pierce Anti-HA Agarose	Thermo Fisher	Cat#26181
Phos-tag acrylamide	Wako	Cat#AAL-107M
Pyrimethamine	Millipore Sigma	Cat#SI 46706
Mycophenolic acid	Millipore Sigma	Cat#M5255
Xanthine	Millipore Sigma	Cat#X7375
6-Thioxanthine	Toronto Research Chemicals	Cat#T385800

(Continued on next page)

Continued

REAGENT or RESOURCE	SOURCE	IDENTIFIER
Critical commercial assays		
Site-directed mutagenesis kit	New England Biolabs	Cat#E0554
NEBuilder HiFi DNA Assembly Master Mix	New England Biolabs	Cat#E2621
DNeasy Blood & Tissue Kit	Qiagen	Cat#69504
RNeasy Mini Kit	Qiagen	Cat#74104
ProtoScript II First Strand cDNA Synthesis Kit	New England Biolabs	Cat#E6560
PDE-Glo Phosphodiesterase Assay	Promega	Cat# V1361
Cyclic GMP Direct ELISA Kit	Arborassays	Cat#K065
Cyclic AMP Direct ELISA Kit	Arborassays	Cat#K065
Pierce BCA Protein Assay kit	Thermo Fisher	Cat#23227
CytoTox 96® Non-Radioactive Cytotoxicity Assay	Promega	Cat#G1780
e-Myco plus kit	Intron Biotechnology	Cat#25237
Experimental models: Cell lines		
Human Foreskin Fibroblasts	ATCC	Cat#CRL-1634
HEK293T	ATCC	Cat# CRL-11268
Experimental models: Organisms/strains		
Parasite lines in Table S1		N/A
Oligonucleotides		
Plasmids listed in Table S2		N/A
Recombinant DNA		
Primers for PCR listed in Table S3		N/A
Software and algorithms		
SnapGene	SnapGene	www.snapgene.com
AxioVision Se64	Carl Zeiss Inc	www.zeiss.com
Gen5	Bioteck	www.bioteck.com
Image Studio	Li-Cor	www.licor.com
Graphpad Prism	Graphpad Software	www.graphpad.com
Image Lab	BIO-RAD	www.bio-rad.com
MaxQuant	Max Planck Institute of Biochemistry	www.maxquant.org
ImageJ	NIH	ImageJ.nih.gov
Phyre2	Imperial College London	www.sbg.bio.ic.ac.uk/~phyre2
MPI Bioinformatics Toolkit	Max Planck Institute for Biology	https://toolkit.tuebingen.mpg.de/
AlphaFold	DeepMind	https://deepmind.com/research/open-source/alphafold

EXPERIMENTAL MODEL AND STUDY PARTICIPANT DETAILS

Parasite and host cell culture

A detailed list of reagents is included in the Key Resources Table. Parasite lines were cultured in human foreskin fibroblast (HFF) cell monolayers maintained in Dulbecco's modified Eagle's medium supplemented with 10% (D10) or 3% (D3) fetal bovine serum, 10 µg/mL gentamicin, and 10 mM glutamine at 37°C with 5% CO₂. All strains and host cell lines were determined to be mycoplasma negative with the e-Myco plus kit. All parasite lines in this study were derived from ME49 parasites expressing Tir1-3FLAG⁸ and are listed in [Table S1](#).

For conditional depletion of mAID fusion proteins, indole-3-acetic acid (IAA) was dissolved in ethanol to yield a 500 mM stock solution and then added to cells at a final concentration of 500 µM. An equivalent volume of ethanol (0.1%) was used as the mock treatment control. To monitor egress, parasites were allowed to infect HFF cells seeded in T25 flasks in the presence of IAA or ethanol at a multiplicity of infection (MOI) 0.75. Images were taken with Nikon eclipse Ts2 inverted phase contrast microscope using 20X objective running the NIS-Elements software at 24, 48, and 72 h post infection (hpi).

METHOD DETAILS

Plasmid construction

A detailed list of cloning reagents and software used in this study are provided in the key resources table. Plasmids, primers, and reagents used for plasmid construction are defined in [Table S2](#). Genomic DNA was isolated using the DNeasy blood and tissue kit. RNA was purified using the RNeasy micro kit and total cDNA was generated with the Protoscript II first strand cDNA synthesis kit. Plasmids were constructed using Q5 polymerase for PCR, commercially available restriction enzymes, a Q5 site-directed mutagenesis kit, or a HiFi DNA assembly cloning kit. Following transformation into *E. coli* DH5 α , transformants were selected on LB agar plates supplemented with 100 μ g/mL ampicillin and screened by colony PCR using Taq polymerase. Positive transformants were then grown for plasmid isolation and Sanger sequencing of the insert (Azbeta Life Sciences, USA). Primers used for sanger sequencing are listed in [Table S3](#).

To generate a plasmid for conditional regulation of PKAc1 (i.e., *p5'PKAc1-mAID-3HA-3'PKAc1, DHFR-TS:HXPRT*), HiFi assembly was performed to introduce ~1.1 kbp homology flanks upstream of *mAID-3HA* and downstream of *DHFR-TS:HXPRT* in the *pTUB1:YFP-mAID-3HA, DHFR-TS:HXPRT* plasmid (Brown et al., 2017). CRISPR/CAS9 plasmids designed to target specific genes were generated from pSAG1:Cas9-GFP, U6:sgUPRT (Shen et al., 2014; Addgene #54467) by replacing the single guide sgUPRT with sgPKAc1, sgPDE2, or sgHXPRT using HiFi assembly. To generate co-expression plasmids (i.e., pETDuet-1:T7:PKAc1_{WT}, T7:PDE2_{CAT} and pETDuet-1:T7:PKAc1_{K65H}, T7:PDE2_{CAT}), PKAc1 was inserted into MCS-1 with an N-terminal 6His-tag and PDE2_{CAT} was cloned into MCS-2 with an C-terminal twin strep-tag of pETDuet-1 using a combination of restriction enzyme digestion and ligation together with HiFi assembly. To generate a catalytically dead form of PKAc1, a K65H point mutation was introduced by site-directed mutagenesis. To generate PDE2 complementation plasmids (i.e., pUPRT::Floxed DHFR-TS*, pPDE2-cPDE2 (X)-2TY, X = WT [wild-type]; CAT. Dead; Group 1 phospho-mimetic [S > D or T > E]; or group 1 phospho-ablative [S > A]), a combination of HiFi assembly reactions and traditional cloning methods were performed. PDE2 was PCR amplified and cloned into pUPRT::Floxed DHFR-TS*, 3'pPDE2-3'PDE2-2TY. The resulting plasmid, pUPRT::Floxed DHFR-TS*, pPDE2-PDE2_{WT} was then amplified by PCR for HiFi assembly reactions with synthetic gene fragments harboring mutations group 1 phospho-mimetic (S > D or T > E) and phospho-ablative (S > A). To introduce mutations (H1944A and D1945A) that produce a catalytically dead PDE2, nucleotides 4,124 - 6,661 (CDS) were sub-cloned into pJET1.2 prior to site-directed mutagenesis. pJET1.2 plasmid harboring H1944A and D1945A were digested with restriction enzymes and cloned into a similarly digested pUPRT::Floxed DHFR-TS*, pPDE2-PDE2_{WT}. To generate plasmids for the expression of recombinant PDE2 (i.e., pCDNA4-PDE2-2Strep wild-type, catalytical dead, phospho-mimetic, and phospho-ablative forms), C-terminal twin strep-tagged PDE2 was PCR amplified and cloned into pCDNA4. The resulting plasmid, pCDNA4-PDE2-2Strep, was digested with restriction enzymes to replace wild-type sequences with synthetic gene fragments containing various point mutations.

Generation of transgenic parasites

All reagents used in transfections are listed in the Key Resources Table. Unless otherwise noted, all transfections were carried out with Tir1-3FLAG parasites in 400 μ L of cytomix (25 mM HEPES [pH 7.6], 10 mM KPO₄, 20 mM KCl, 5 mM MgCl₂, 2 mM EDTA) supplemented with 150 nM calcium chloride (CaCl₂), 5 mM glutathione (GSH), and 2 mM adenosine triphosphate (ATP) and 50 μ g tagging plasmid or 20 μ g DNA amplicon and 50 μ g CRISPR/CAS9 plasmid. Following transfection, parasites were passaged three times in the presence of drug prior to isolation by limiting dilution. All clones were validated by PCR and expression of mAID-3HA, 2Strep, and 6His tags were verified by IFA and/or Western blot analysis. GCaMP expression was confirmed using live cell imaging. Primers used for diagnostic PCRs are shown in [Table S3](#). All parasite lines generated in this study are listed in [Table S1](#).

Knockout lines for the ACs were generated by CRISPR/Cas9 utilizing dual sgRNAs targeting regions adjacent to both the start and stop codons simultaneously, was introduced into the ME49 TIR1-3FLAG parental line to generate the Δ AC α s mutant. Plasmids containing the dual sgRNAs (pSAG1:Cas9-GFP, dual U6:sgAC α s) were constructed and co-transfected with DNA amplicons harboring a LoxP-flankedDHFR-TS selection marker, flanked by 40-bp homologous arms corresponding to sequences near the AC α s-targeting sgRNAs. Transfected parasites were selected using 3 μ M pyrimethamine, followed by limiting dilution for cloning and validation.

To generate a transgenic line for conditional regulation of PKAc1 (i.e., PKAc1-mAID-3HA), parasites were co-transfected with a tagging plasmid (*p5'PKAc1-mAID-3HA-3'PKAc1, DHFR-TS:HXPRT*) and CRISPR/CAS9 plasmid targeting PKAc1 (pSAG1:Cas9-GFP, U6:sgPKAc1). To generate a transgenic line for regulated degradation of PDE2 (i.e., PDE2-mAID-3HA), a DNA amplicon generated from pTUB1:YFP-mAID-3HA, DHFR-TS:HXPRT was co-transfected into parasites with a CRISPR/CAS9 plasmid targeting PDE2 (pSAG1:Cas9-GFP, U6:sgPDE2). Transfectants were selected using 25 μ g/mL mycophenolic with 25 μ g/mL xanthine. To C-terminally tag PDE2 with a twin strep tag in the PKAc1-mAID-3HA line (i.e., PKAc1-mAID-3HA, PDE2-2Strep), parasites were co-transfected with a DNA amplicon generated from p2Strep, DHFR* and pSAG1:Cas9-GFP, U6:sgPDE2. Following transfection, parasites were maintained in 3 μ M pyrimethamine. To generate a line for monitoring calcium in PKAc1-mAID-3HA and PDE2-mAID-3HA lines (i.e., PKAc1-mAID-3HA, GCaMP and PDE2-mAID-3HA, GCaMP), parasites were co-transfected with an amplicon derived from a plasmid containing the calcium reporter protein pNJ-26 (Fu et al., 2021) together with CRISPR plasmid designed for integration into the HXPRT locus (pSAG1:Cas9-GFP, U6:sgHXPRT). Transfectants were FACs sorted with Sony SH800S cell sorter for CAS9-GFP expression followed by selection with 200 μ g/mL 6-thioxanthine. To generate PDE2 complemented lines (PDE2-mAID-3HA, GCaMP, cPDE2 [X]-2TY; X = WT (wild-type); H1944A & H1945A; S40D, S53D, S271D, S314D, & S315D; and S40A, S53A, S271A,

S314A, & S315A), PDE2-mAID-3HA, GCaMP parasites were co-transfected with PDE2 complementation plasmids harboring no mutations (*pUPRT::Floxed DHFR-TS**, *pPDE2:PDE2-2TY_{WT}*) or mutations listed above (*pUPRT::Floxed DHFR-TS**, *pPDE2:PDE2-2TYX*); and a CRISPR plasmid targeting the UPRT locus (*pSAG1:CAS9-GFP*, *U6:sgUPRT*). Transfectants were selected using 3 µM pyrimethamine prior to isolation by limiting dilution.

Western blotting

Parasites were harvested by centrifugation at 400 x g for 10 min at 4°C and lysed using CellLytic M buffer supplemented with Benzonase and protease inhibitor cocktail. Lysates were solubilized in Laemmli buffer followed by heating, separated on 10 or 12% SDS-PAGE gels, and transferred to nitrocellulose membranes. Blots were blocked for 1 h in non-fat milk in PBS (5% wt/vol), probed with primary antibodies (mouse monoclonal or rabbit polyclonal α-HA antibodies, 1:1000; mouse monoclonal α-strep tag antibodies, 1:5000; and rabbit monoclonal α-aldolase antibodies, 1:1000) overnight, and then incubated with goat IR dye-conjugated secondary antibodies (1:10,000) for 1 h. All blots were imaged using the Odyssey infrared imaging system and analyzed using the image studio software.

Fluorescence microscopy

HFF cells were seeded on glass coverslips in 24-well plates and grown to 90–100% confluence prior to infection. Cells were infected with freshly harvested parasites at MOI of 0.5–1, treated with IAA (500 µM) or diluent (0.1% ethanol) for 1 h, and fixed at 24 hpi with 4% formaldehyde for 10 min. Parasite infected cells were permeabilized with 0.1% Triton X-100 for 10 min and blocked with 3% BSA (wt/vol) supplemented with 0.1% Tween 20 in PBS for 30 min. Cells were then incubated with primary antibodies in blocking buffer for 1 h, washed with PBS, and incubated with Alexa Fluor-conjugated secondary goat antibodies (1:1000) for 1 h followed by Hoechst 33342 dye for 5 min. Coverslips were washed 3X with PBS and 1X with H₂O prior to mounting with Prolong gold antifade reagent. Images were captured with a 100X oil objective on an Axioskop 2 MOT Plus wide-field fluorescence microscope (Carl Zeiss, Inc.) running AxioVision LE64 software (Carl Zeiss, Inc.).

Plaque formation assay

Two hundred freshly egressed parasites were used to infect HFF cells seeded six well plates in duplicate or triplicate in the presence of IAA (500 µM) or diluent (0.1% ethanol). Following growth for 14 days, cells were fixed with 100% ethanol for 5 min, washed with H₂O, and stained with 0.1% crystal violet for 10 min. Images were taken using a Bio-Rad ChemiDoc MP imager and analyzed using the ImageJ software (<https://imagej.nih.gov/ij/>).

Purification of recombinant PDE2 (rPDE2)

Recombinant C-terminal twin strep-tagged PDE2 (rPDE2) was purified from transiently transfected HEK-293T cells as described in previously⁶⁰ with slight modifications. Unless otherwise noted, adherent HEK293T cells were maintained in D10 at 37°C with 5% CO₂. Stock polyethylenimine (PEI) solutions (10 mg/mL in H₂O) were diluted to 1 mg/mL, adjusted to pH 7, and filter sterilized prior to use. For one transfection, 50 µg DNA was incubated with 75 µL PEI for 30 min at room temperature (RT) in 5 mL serum free DMEM and then added adherent HEK293T cells (90% confluent) in 15 mL DMEM supplemented with 2% FBS. The cells were then cultured for 48 h at 37°C with 5% CO₂ prior to harvesting.

To purify rPDE2, four 150 mm tissue culture dishes were transfected as described above. Following expression for 48 h, the cells were washed with PBS, incubated with lysis buffer (PBS supplemented with 1% n-Dodecyl-Beta-Maltoside (DDM), 1 mM Tris(2-carboxyethyl)phosphine (TCEP), and protease inhibitor cocktail), and dislodged with glass beads. The supernatant was sonicated (30 pulses, 50% duty, and an output level 2, Branson Sonifier 250), pelleted at 13,000 x g for 15 min at 4°C remove debris, and passed through a 0.45 µm filter for affinity purification with using Streptactin XT Sepharose. rPDE2 was quantified using Pierce BCA protein assay kit and stored in 20% glycerol at –20°C for up to 1 week. All protein preparations were assessed for total protein and identity using SDS-PAGE gels with Instant Blue stain (Coomassie brilliant blue stain) and α-Strep Western blot analysis.

PDE assays

Parasites were liberated from HFF cell monolayers by scraping and syringe lysing through a 25G needle. Following centrifugation at 400 x g for 10 min 4°C, pellets were resuspended in CellLytic M supplemented with Benzonase and protease inhibitor cocktail and incubated end-over-end for 15 min. Lysates were centrifuged at 13,000 x g for 10 min at 4°C to remove debris and supernatants were added to 30 µL α-HA conjugated beads to immunoprecipitated PDE2. After binding end-over-end for 1 h, beads were washed 3X with wash buffer (50 mM Tris and 150 mM NaCl) and then resuspended in 70 µL of wash buffer. Ten percent of immunoprecipitated PDE2 sample was reserved for α-HA Western blot analysis and the remaining sample was split equally for PDE assays using cAMP or cGMP as a substrate.

To measure cNMP hydrolysis, endpoint assays were performed using the PDE-Glo phosphodiesterase assay according to manufacturer's guidelines with slight modifications. Reactions were initiated by centrifugation of either cAMP or cGMP into wells of a 96-well half-area flat-bottom white polystyrene plate containing immunoprecipitated PDE2 or α-HA conjugated beads alone diluted in reaction buffer (1 µM cAMP or 10 µM cGMP in 25 µL total reaction volume) and incubated at 30°C for 1 h. For assays with purified rPDE2, 0.3 µg protein was added to reaction buffer containing 1 µM cAMP and incubated at 30°C for 3 h and 40 min. All reactions

were terminated by the addition of 12.5 μ L termination buffer followed by incubation with 12.5 μ L detection buffer for 20 min and 50 μ L Kinase-Glo reagent for 10 min. Luminescence was measured using a CytaGlo 3 (BioTek) multimode plate imager running Gen5 software (BioTek). Background Relative Light Units (RLU) values from reactions with α -HA conjugated beads alone were subtracted from RLU values from reactions with PDE2 for each cNMP tested.

cAMP and cGMP ELISA assays

HFF cell monolayers were infected with parasites at an MOI of 0.75. At 3 dpi, infected cell monolayers were treated with IAA (500 μ M) or diluent (0.1% ethanol) for 4 h and washed with IC buffer (142 mM KCl, 5 mM NaCl, 1 mM MgCl₂, 5.6 mM d-glucose, 2 mM EGTA, 25 mM HEPES, pH 7.4) supplemented with IAA or ethanol. Parasites were then purified in IC buffer and pellets were stored at -80°C until use. IAA and ethanol treated samples were normalized based on protein content determined by the Pierce BCA protein assay. Each sample was adjusted using the sample diluent provided in the cyclic AMP and GMP Direct ELISA kits from Arborassays and cNMPs were measured following the manufacturer's instructions.

PhosTag gels

Rosetta (DE3) cells harboring co-expression plasmids were grown in the presence of ampicillin and chloramphenicol at 37°C with shaking to an optical density at 600 nm (OD₆₀₀) of 0.6–0.8. Cultures were then chilled on ice and induced with 0.1 mM isopropyl β -D-1-thiogalactopyranoside (IPTG) for 20 h at 16°C with shaking. Cells were harvested by centrifugation at 4000 xg at 4°C and lysed with CellLytic B supplemented with protease inhibitor cocktail. Following centrifugation to remove cell debris, supernatants were added to Streptactin resin and allowed to bind end-over-end for 1 h. The resin was washed 3X with wash buffer and transferred evenly into tubes with and without Lambda phosphatase. Phosphatase reactions were performed at 30°C for 1 h and subsequently terminated by the addition of Laemmli buffer followed by heating at 95°C–100°C for 5 min. Protein samples were run on 12% SDS-PAGE gels supplemented with 50 μ M Phos-tag reagent and without Phos-tag reagent and stained with InstantBlue Coomassie stain. Images were taken using a Bio-Rad ChemiDoc MP imager.

Identification of PDE2 phosphosites

Parasites were used to infect HFF cell monolayers at an MOI of 0.8 in the presence of AA (500 μ M) or diluent (0.1% ethanol) and were allowed to grow for 3 days. Cells were washed with PBS and parasites were purified using standard protocols. Pellets were resuspended in CellLytic M buffer supplemented with 5 mM EDTA, protease inhibitor cocktail, and PhosSTOP and incubated end-over-end for 15 min followed by sonication on ice for 15 pulses (30% duty cycle, output control 4, Branson sonifer 250). Following centrifugation at 4000 xg for 20 min at 4°C, supernatants were added to streptactin resin and allowed to bind end-over-end for 2 h at 4°C. The resin was washed 5X with wash buffer and then solubilized in Laemmli buffer with heating. Western blot analysis with mouse monoclonal α -Strep tag antibodies were performed to assess PDE2 protein levels. Equivalent amounts were run on 10% SDS PAGE gels, stained with Sypro Ruby according to the manufacturer's guidelines, and bands corresponding to PDE2-2Strep were excised.

Gel bands were washed in 100 mM Ammonium Bicarbonate (AmBic)/Acetonitrile (ACN) and reduced with 10 mM dithiothreitol at 50°C for 30 min. Cysteines were alkylated with 100 mM iodoacetamide in the dark for 30 min in room temperature. Gel bands were washed in 100 mM AmBic/ACN prior to adding 500 ng trypsin for overnight incubation at 37°C. Supernatants were saved into a new tube. The gel bands washed at room temperature for 10 min with gentle shaking in 50% ACN/5% FA, and supernatant was saved to peptide solution. Wash step was repeated each by 80% ACN/5% FA, and 100% ACN, and all supernatant was saved then subject to the speedvac dry. After lyophilization, peptides were reconstituted with 0.1% FA in water and injected onto a Neo trap cartridge coupled with an analytical column (75 μ m ID x 50 cm PepMapTM Neo C18, 2 μ m). Samples were separated using a linear gradient of solvent A (0.1% formic acid in water) and solvent B (0.1% formic acid in ACN) over 120 min using a Vanquish Neo UHPLC System coupled to an Orbitrap Eclipse Tribrid Mass Spectrometer with FAIMS Pro Duo interface (Thermo Fisher Scientific).

The data was queried for protein identification against the custom database, 'Toxoplasma gondii ME49' plus the PDE2-Strep sequence using MaxQuant v2.1.4.⁶¹ The following modifications were set as search parameters: peptide mass tolerance at 20 ppm, trypsin digestion cleavage after K or R (except when followed by P), 2 allowed missed cleavage sites, carbamidomethylated cysteine (static modification), and oxidized methionine, deaminated asparagine/glutamine, protein N-term acetylation, and phosphorylated serine, threonine, and tyrosine (variable modification).

Egress assays

Natural egress at a late stage of intracellular growth was measured using the CytoTox 96 Non-Radioactive Cytotoxicity Assay (Promega) according to the manufacturer's protocol. Briefly, host cells split in 96-well plates were infected with different parasite strains at a multiplicity of infection (MOI) of 1, and subsequently incubated for 0, 24 h, 48 h, 96 h with or without 500 μ M IAA. At each time-point, medium was replaced with 50 μ L extracellular (EC) buffer (5 mM KCl, 142 mM NaCl, 1 mM MgCl₂, 1.8 mM Ca²⁺, 5.6 mM D-glucose, 25 mM HEPES, pH 7.4) containing \pm 500 μ M IAA and incubated for an additional 6 h. At the end of 6 h, 50 μ L of cell supernatant was harvested and mixed with 50 μ L of assay buffer and substrate for 30 min at room temperature. The reaction was stopped with 50 μ L stop solution, and absorbance was measured at 490 nm. LDH release was calculated as a percentage of maximal release (post-Triton treatment of non-infected cells).

For premature egress experiments, parasites were cultured in HFF cell monolayers for two days and then treated with IAA (500 μ M) or diluent (0.1% ethanol) overnight. Parasites were then purified from HFF cells in EC buffer (5 mM KCl, 142 mM NaCl, 1 mM MgCl₂, 1.8 mM CaCl₂, 5.6 mM d-glucose, 25 mM HEPES, pH 7.4) supplemented with IAA or ethanol and added to fresh HFF cells monolayers attached to 35 mm glass bottom dishes in prewarmed EC buffer with IAA or ethanol. Experiments were performed in duplicate and 10–50 invaded parasites were quantified for egress in each dish. For calcium traces, GCaMP fluorescence intensities from 10 individual parasites treated with or without IAA from different experiments were measured over a 5 min time frame. Relative intensity of GCaMP fluorescence fold change (f/f_0) represents a ratio GCaMP fluorescence at each time point (f) vs. GCaMP fluorescence prior to invasion (f_0).

For performing egress assays using GCaMP expressing parasites, HFF cells were seeded in 35 mm glass bottom dishes were infected with an MOI of 0.5–0.75. Parasite infected cells were treated with IAA (500 μ M) or diluent (0.1% ethanol) at 24 hpi and H89 was added at concentrations indicated in figure legends at 32 hpi. At 52 hpi, infected cell monolayers were washed 3X with EC buffer supplemented with IAA or ethanol prior to the addition of 250 μ M Zaprinast or 1 μ M ionomycin at T₀. Images were taken using tiling and egressed vacuoles were quantified (at least 15 vacuoles) over 30 min for each tile and averaged for each time point. For calcium traces, GCaMP fluorescence intensities from three individual vacuoles treated with IAA or diluent from different experiments were averaged for each time point. Relative intensity of GCaMP fluorescence fold change (f/f_0) represents the average ratio GCaMP fluorescence at each time point (f) vs. GCaMP fluorescence at the addition of agonist (f_0) from at least three independent experiments.

For time lapse microscopy experiments, alternating phase and fluorescence images were taken at 37°C on a Zeiss AxioObserver Z1 (Carl Zeiss, Inc) equipped with an ORCA-ER digital camera (Hamamatsu Photonics) and a 40X oil EC Plan-Neofluar objective (N.A. 0.50) running the Zen software 2.6 blue edition (Zeiss).

QUANTIFICATION AND STATISTICAL ANALYSIS

Statistics

Statistical analyses were performed in GraphPad Prism software version 9.0.0. All data were analyzed using Student's t-tests and comparisons were considered statistically significant when p values were less than 0.05. Experiment-specific statistical information is provided in the figure legends.